

UNIVERSITY OF SOUTHAMPTON

FACULTY OF SCIENCE

PHYSICS

SURFACE CHARGE DECAY OF INSULATORS WITH TRAPS

by

Dariush Moayyed-Mohseni

Submitted for the degree of Master of Philosophy

September 1988

TO MY FAMILY

Acknowledgements

This work was carried out under the supervision of Dr B. H. Blott to whom I am very grateful for the invaluable advice given to me over many years and in particular on the completion of this thesis. I would like to express my sincere thanks to Dr K. S. Thomas of Computer Science Department for all his help. I would also like to thank Dr G. J. Daniell for all the discussions we had. My thanks go to N. L. Adcock for producing the experimental results. I am grateful to Dr M. Taylor for providing the computer facilities. I also feel indebted to Mr M. Hill for providing all the computer softwares and for his invaluable advice. My thanks also go to colleagues in the Upper Atmospheric Group for their assistance.

My sincere thanks to my mother, my late father, my brother and my sisters not only for their financial support, but also for their encouragement and moral support.

I also would like to express my deepest gratitude to my friend Nika for her continuous encouragement, patience and understanding without whom everything seemed lost.

I would like to thank members of staff particularly Maureen for not only being helpful but, also very friendly.

Contents

	Page
Chapter 1: INTRODUCTION	
1.1 General background	1
1.2 Conduction mechanisms in polymers	4
Chapter 2: THE PHYSICAL MODEL	
2.1 Injection process	6
2.2 Transport equations	7
2.3 Formulation of the equations in reduced quantities	9
2.4 Boundary and initial conditions	10
2.5 Approximation methods for the reduced transport equations	11
2.6 Finite difference approximations to derivatives	12
2.7 Characteristics and hyperbolic equations	13
2.8 The Courant-Friedrich-Lowy (C.F.L) condition	14
2.9 Finding the characteristics for equations	15
2.10 Solution of the reduced partial differential equations	17
2.11 Calculation of the surface potential	18
2.12 Programming of the explicit Lax-Wendroff schemes	19

Chapter 3: RESULTS AND DISCUSSION

3.1	Results	21
3.1.1	Experimental results	21
3.1.2	Curve fitting techniques	21
3.1.3	Evaluation of the transport parameters	23
3.1.4	The von Berlepsch's model	24
3.2	The derived results	25
3.2.1	The electric field strength	25
3.2.2	The free charge density	25
3.2.3	The trapped charge density	26
3.2.4	The total charge in the sample	26
3.2.5	Other transport parameters	27
3.3	Discussion	28
3.4	Conclusion	30
	References	32

UNIVERSITY OF SOUTHAMPTON

ABSTRACT

FACULTY OF SCIENCE

PHYSICS

Master of Philosophy

SURFACE CHARGE DECAY OF INSULATORS WITH TRAPS

by

Dariush Moayyed-Mohseni

The aim of this research was to develop an understanding of the surface potential decay of corona charged insulating materials. The experimental results for polyethylene samples showed a remarkable crossover of the surface potential profiles.

A quantitative theoretical description of the experimental results based on the concept of hopping transport of charge carriers between traps of identical energy in the sample was used. A computer programme based on a finite difference scheme was developed to solve the resultant transport equations. The solution was extended to cover several transit times of the charge passage in the sample. The transport and trapping parameters i.e. the injection factor, the charge carrier mobility, the trapping time before release and the free time before capture were determined by curve fitting techniques. The fitted transport and trapping parameters were used to determine the free charge distribution, the trapped charged distribution and the electric field in the sample. The derived transport and trapping parameters were field dependent: the value were for the trap energy 0.97 eV at field 83.3 MV/m to 1.136 eV at 16.4 MV/m and for the trap concentration $5.35 \times 10^{23} \text{ m}^{-3}$ at 83.3 MV/m to $0.45 \times 10^{23} \text{ m}^{-3}$ at 16.4 MV/m. The Poole-Frenkel field lowering factor was $(3.5 \pm 0.3) \times 10^{-5} \text{ CV}^{1/2} \text{ m}^{1/2}$ in good agreement with theory $(5.04 \times 10^{-5} \text{ CV}^{1/2} \text{ m}^{1/2})$.

CHAPTER 1: INTRODUCTION

1.1 General Background

In recent years considerable importance has been given to the study of insulating materials due to their numerous applications in different industries. The use of photoconductive insulators in electrophotography or use of insulators in the cable industry are two examples. The optimisation of their performance requires the investigation of the charge transport processes in the material. Surface-charge decay measurements have proven to be a convenient method for studying the processes involved. In this technique a thin film of an insulator (e.g. polyethylene) is charged on one surface either by corona discharge, ion bombardments or contact charging while the opposite surface is laid on a grounded electrode. The surface potential decay of the charged surface is then observed over a period of time using an electrostatic probe. Such decay profiles have been reported by many investigators (ref 1-29). Some have found that the surface potential decays faster for higher initial voltages, that there is an apparent levelling off in the curves for low initial potentials, and that the decay curves for various potentials cross each other at finite time after charging. Many authors have proposed physical models which attempt to account for this phenomenon.

Batra and co-workers (ref 31-32) have developed various theories for surface potential decay; their work assumes space charge conduction, but they do not include the effect

of partial instantaneous injection and trapping of the carriers.

Wintle (ref 30, 33 and 34) has speculated on various explanations for the observed features of polyethylene decay curves. He has developed theories that include field-dependent mobilities of various forms as well as trapping. None of these models can account for the cross over effect. He derives some interesting results assuming a field-dependent depth of penetration of the initial charge. However Batra (ref 35) has shown that this model cannot explain the cross over phenomenon.

Sonnostine and Perlman (ref 36) considered field dependent mobilities and both partial instantaneous and time dependent injection, but have not considered the effect of trapping and release of charges from the traps in the sample.

Robins (ref 46) assumed a steady-state situation, where no time dependent change for charge density and the electric field can occur. He has not considered charge trapping in the sample, hence his analytically derived solution for the surface potential decay only applies to high initial surface potential where no trapping occurs.

Chudleigh (ref 2) has considered the effect of trapping and release, but has not considered partial injection from the surface and his numerically solved model does not cover times beyond the transit time of charge passage through the whole sample.

von Seggern (ref 7) suggested a model based on surface and bulk traps and considered time dependent surface injection, but again his model does not cover times greater than the transit time.

Campos and Giacometti (ref 12) have assumed instantaneous injection and trapping of charges but their model does not allow liberation of the charges from traps.

Arkipov and co-workers (ref 40) considered a model characterised by a system of traps whose energies are distributed within a wide region into the band gap. In this model they considered partial injection of charges from the surface but, in order to solve the transport equations analytically, they had to resort to approximation methods. Consequently when the injection factor $\gamma \rightarrow 1$ (i.e. ratio of injected charge to total surface charge $\rightarrow 1$), their method became very inaccurate.

von Berlepsch (ref 24-26) considered a model in which surface and bulk traps exist and he assumed partial injection of charges from the surface, but he had to use approximation methods in order to find analytical solutions for the transport equations. His model does not allow times greater than the transit time.

Detection of surface and charge traps by von Seggern (ref 37-38) and Mizutani and co-workers (ref 45) and measurements of their positions and energies in the sample have lent credibility to the models which are based on surface and

bulk traps.

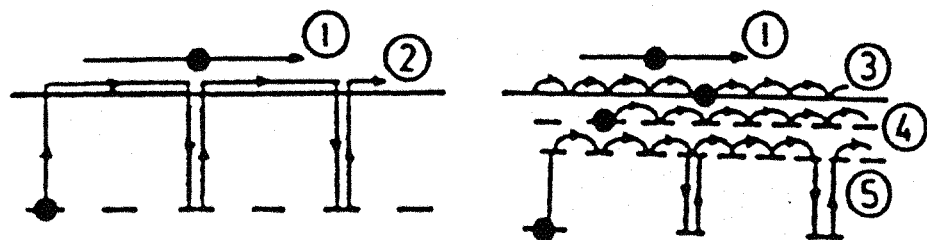
The aim of this study is to provide solutions for the transport equation based on the considerations that partial injection of charge from the surface occurs and that the sample has surface and bulk traps. It is also desirable to extend the solutions to times greater than the transit time, and to find the relevant parameters by fitting the theoretically produced surface potential decay curves to the experimental results. But before proceeding any further it is instructive to give a brief review of the possible conduction mechanisms in polymers.

1.2 Conduction mechanisms in polymers

Polymers are not the simple covalent or ionically bonded crystals of conventional solid-state physics. For example polyethylene is a covalently-bonded, long chain molecule, where the chains are weakly bonded by van der Waals' forces to form a semicrystalline solid: i.e a mixture of crystalline and amorphous parts. The carrier mobility in these materials is very low and so there are difficulties in the use of band theory. These difficulties arise from the fact that two of the conditions in the the band model, namely the weak electron-lattice interaction and the extended nature of the electron states, are violated because of the strong intra-molecular localisation of the electron states and the weak electronic coupling between molecules which exist in these materials (ref 42). An alternative model based on electron hopping through the states is more applicable (ref 41). A carrier can move from one chain to

another by jumping over the potential barrier which exists between the two chains. However, the bonding between molecules of one chain is strong and covalent, and electron-lattice interaction rather weak therefore a band scheme is appropriate for a PE chain (ref 39). The band structure of a PE chain has been modelled theoretically and the calculated band gap of 7.6 eV is in good agreement with the experimental value of about 8 eV (ref 39). A sample of PE consists of a large number of PE chains and carriers move across the sample with repeating band conduction along a PE chain and hopping to the next chain alternately. In a semicrystalline material like PE, carriers travel through crystalline parts and amorphous parts, hence several different possible transport mechanisms may exist in parallel. Furthermore the existence of carrier traps in the material (which may be caused by defects, impurities, etc...) adds new complications to the transport phenomenon in PE. These mechanisms are shown in Fig 1.1. However, many authors (see for example ref 9 and ref 26) consider the thermally-activated hopping to be the dominant transport mechanism in PE. Assuming the band model with a band gap of 8 eV for PE, the energy level diagram of PE is shown in Fig 1.2. The trap levels are caused by defects, unstable oxidation products, stable oxidation products, crosslinks and antistatic agents (ref 39). For a thorough discussion of the transport mechanisms in polymers see for example Kao and Hwang (ref 41), M. Ieda (ref 39) and G.G.Roberts *et al.* (ref 42).

Conduction Band



1. Trap-Free Band Conduction
2. Trap-Controlled Band Conduction
3. Brownian Motion
4. Tunnel Hopping
5. Thermally Activated Hopping

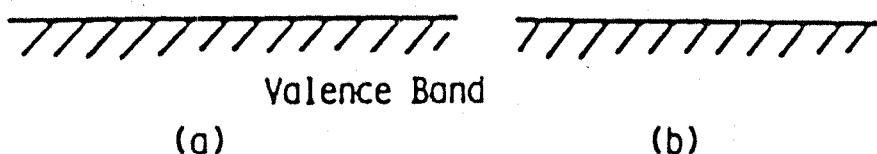


Fig. 1.1: Carrier transport mechanisms:

(a) single crystal,

(b) amorphous material.

[After M. Ieda ref. 39].

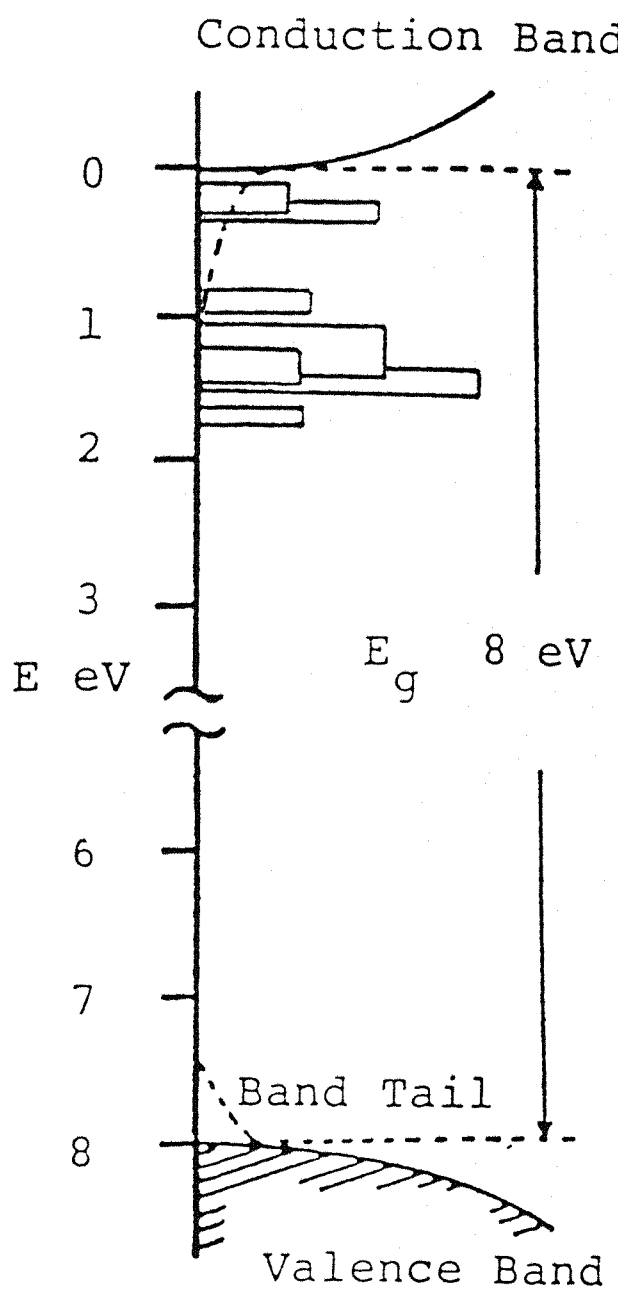


Fig. 1.2: Energy level diagram of carrier traps in PE. [After M. Ieda ref. 39].

CHAPTER 2 : THE PHYSICAL MODEL

2.1 Injection process

Consider a thin insulator in a plane-parallel geometry of thickness L and dielectric constant $\epsilon\epsilon_0$ with one surface in contact with a grounded electrode and the other free. At time $t=0$, a surface charge of density σ_0 is deposited "instantaneously" on the free surface from a corona discharge unit. Instantaneous charging means that the charge is deposited before a significant portion of it moves into the bulk. The charge is deposited in the form of positive (or negative) ions. These ions may remain stable on the surface or, depending on the polarity of the incident ions, the surface states of the insulator may be ionised producing acceptors or donors. Consequently we assume that a part of the total deposited charge $\gamma\sigma_0$, where $0 \leq \gamma \leq 1$, is instantaneously injected from the surface states and the remaining part $(1-\gamma)\sigma_0$ is trapped in the surface states for a longer period of time than the duration of the experiment. For the purpose of modelling the injection process we exclude the possibility of direct molecular ion migration in the insulator. Transport of charge from the surface states into the bulk requires hole or electron transfer into the valence or conduction band states. In polymer structures like polyethelyne, the bands will be sets of localised states energetically close together. Electron or hole transport is possible by activated hopping from one localised state to another. The tails of bands are extended into the band gap to give a "mobility edge". This model is

applicable for transport phenomena in amorphous materials. In addition to the localised states, it is considered that a set of deeper traps, with a single energy level E_t , exists in the band gap and are uniformly distributed across the bulk. These traps may be characterised by means of T_t and T_f for carrier trapping time before release and free carrier time before capture, respectively.

Once the carriers are in the bulk, they move towards the opposite grounded electrode with mobility μ under their self induced electric field. While moving, some of them are captured by these traps and then subsequently released into the transport states. So at any time after the injection some trapped charge exists in the sample (Fig.2.1).

2.2 Transport equations

To simplify the model, the following assumptions are made:

- 1) Part of the total charge (σ_0) deposited at the surface ($\gamma\sigma_0$), is assumed to be injected instantaneously into the bulk and the remainder $(1-\gamma)\sigma_0$, is assumed to stay at the surface states.
- 2) The transport of injected carriers is assumed to occur by activated hopping between localised states under the influence of their own electric field.
- 3) Injection of counter charges into the sample from the substrate is assumed to be insignificant compared to charge injection from the surface.
- 4) Contributions by diffusion, Ohmic conduction, thermal generation are assumed to be insignificant

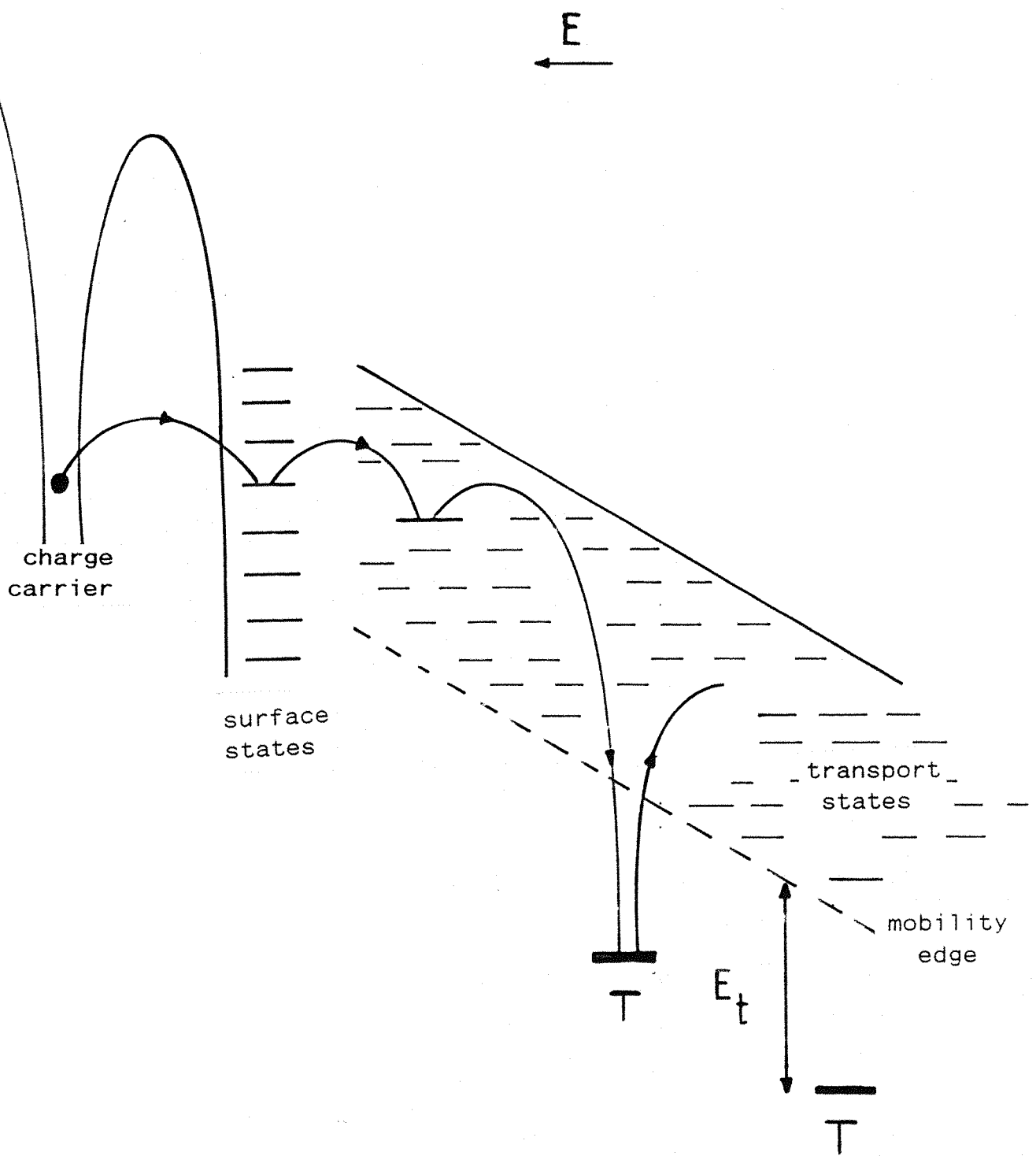


Fig. 2.1: Scheme for charge transport from ions into surface and bulk states under self induced electric field. The traps have trapping time T_t and release time T_f . The activation energy for release is E_t . [Similar to G. Lederer et al., ref. 10].

5) During the passage of carriers through the sample it is considered that the carriers are repeatedly captured and released by traps which are situated in a single energy level, characterised by T_f , the mean free time before capture and T_t , the mean capture period before release. Transport between trapped states is characterised by carrier mobility μ . With these assumptions we can now write the transport equations. In one dimension we have,

The conduction current $J_c(x,t)$:

$$J_c(x,t) = \rho_f(x,t) \mu E(x,t). \quad (1)$$

where $\rho_f(x,t)$ is the free charge density,

$E(x,t)$ is the electric field strength,

μ is the carrier mobility.

The displacement current density $J_d(x,t)$:

$$J_d(x,t) = \epsilon \epsilon_0 \partial E(x,t) / \partial t. \quad (2)$$

The total current density $J(t)$ is equal to the sum of $J_c(x,t)$, and $J_d(x,t)$, and furthermore for an open circuit configuration $J(t)=0$. Hence,

$$\mu \rho_f(x,t) E(x,t) + \epsilon \epsilon_0 \partial E(x,t) / \partial t = 0. \quad (3)$$

For trapping centres located at a single energy level, the rate of change of trapped charge density is:

$$\partial \rho_t(x,t) / \partial t = \rho_f(x,t) / T_f - \rho_t(x,t) / T_t. \quad (4)$$

where $\rho_f(x,t) / T_f$ represents the rate of increase of $\rho_t(x,t)$ due trapping of free carrier and $\rho_t(x,t) / T_t$ represents the rate of decrease of $\rho_t(x,t)$ due to release of trapped carriers.

The surface potential is given by:

$$V(t) = \int_0^L E(x, t) dx. \quad (5)$$

The initial surface potential is :

$$V_0 = \sigma_0 L / \epsilon \epsilon_0 \quad (6)$$

2.3 Formulation of the equations in reduced quantities

The computational stage of all numerical methods for solving problems of any complexity generally involves a great deal of arithmetic. It is usual therefore to arrange, whenever possible, for one solution to cover a variety of different situations. This can be done by expressing all equations in terms of non-dimensional variables. In this particular case we can write:

$$x^* = x / L, \quad t^* = t / t_0, \quad T_f^* = T_f / t_0, \quad T_t^* = T_t / t_0, \\ \rho_f^*(x^*, t^*) = \rho_f(x, t) L / \sigma_0, \quad \rho_t^*(x^*, t^*) = \rho_t(x, t) L / \sigma_0, \\ E^*(x^*, t^*) = E(x, t) L / V_0, \quad V^*(t^*) = V(t) / V_0.$$

The variables on the left side of the equations are the non-dimensional equivalent of the transport equations. Here t_0 is the transit time of a carrier at the leading edge of the charge distribution in the absence of trapping (ref. Batra) and is related to the carrier mobility μ by :

$$t_0 = L^2 / \mu V_0. \quad (7)$$

The equivalent transit time in the reduced model is $t^* = 1$.

Substituting the dimensionless variables into the transport equations (1-6) we have:

$$\rho_f^*(x^*, t^*) E^*(x^*, t^*) + \partial E^*(x^*, t^*) / \partial t^* = 0, \quad (8)$$

$$\partial E^*(x^*, t^*) / \partial x^* = \rho_f^*(x^*, t^*) + \rho_f^*(x^*, t^*), \quad (9)$$

$$\partial \rho_t^*(x^*, t^*) / \partial t^* = \rho_f^*(x^*, t^*) / T_f^* - \rho_t^*(x^*, t^*) / T_t^*, \quad (10)$$

$$V^*(t^*) = \int_0^1 E^*(x^*, t^*) dx^*. \quad (11)$$

2.4 Boundary and initial conditions

Equations (8-11) are subject to the following boundary and initial conditions :

At $t^* = 0$, charges are injected into the sample so there is a surge of free carriers into the sample. Hence,

$$\rho_f^*(x^*, 0) = \gamma \delta(x^*) \quad 0 \leq x^* \leq 1 \quad (12)$$

where $\delta(x^*)$ is the Dirac delta function. Recall that:

$$\int_{-\infty}^{+\infty} \delta(x) dx = 1.$$

and γ is the ratio of injected charge to total surface charge, so:

$$0 \leq \gamma \leq 1.$$

The electric field inside the sample is :

$$E^*(x^*, 0) = 1. \quad 0 < x^* \leq 1 \quad (13)$$

and on the free surface of the sample :

$$E^*(0, t^*) = 1 - \gamma. \quad (14)$$

Prior to injection of carriers, there is no trapped charge in the sample, so

$$\rho_t^*(x^*, 0) = 0. \quad 0 \leq x^* \leq 1 \quad (15)$$

2.5 Approximation methods for the reduced transport equations

There appears to be no analytical solutions to these equations with the given boundary conditions, so approximation methods must be used. Analytical approximation methods often provide useful information about the variables and a few authors have used these methods (ref. 40, 25). But their solutions are limited to less than the transit time of the carrier passage. Of the numerical approximation methods available for solving partial differential equations those employing finite differences or finite elements are more frequently used, and are more applicable to these problems. In the present case the finite difference approximation method is used. Before outlining this method however, it is necessary to mention that finite difference methods are "approximate" in the sense that derivatives at a point are approximated by difference quotients over a small interval, i.e. if U is a function of x and y , then $\partial U / \partial x$ is replaced by $\delta U / \delta x$ where δx is small and y is constant. The data of the experiment are inevitably subject to errors of measurement, and all arithmetical calculations are subject to a finite number of significant figures, and so even complete analytical solutions are subject to uncertainty in numerical comparison with experiment.



2.6 Finite difference approximations to derivatives

Assume U is a function of the independent variables x and t . We subdivide the $x-t$ plane into sets of equal rectangles with sides $\delta x=h$, $\delta t=k$, as shown in Fig.2.2, and let the co-ordinates (x,t) of the mesh point R be :

$$x=ih ; \quad t=jk,$$

where i and j are integers. The value of U at R is

$$U=U(ih,jk)=U_{i,j}.$$

Then the derivatives for forward-differences are:

$$\frac{\partial U}{\partial x} \cong U_{i+1,j} - U_{i,j} / h, \quad (16)$$

$$\frac{\partial U}{\partial t} \cong U_{i,j+1} - U_{i,j} / k, \quad (17)$$

and for backward-differences we have:

$$\frac{\partial U}{\partial x} \cong U_{i,j} - U_{i-1,j} / h, \quad (18)$$

$$\frac{\partial U}{\partial t} \cong U_{i,j} - U_{i,j-1} / k, \quad (19)$$

and for central-differences we have:

$$\frac{\partial U}{\partial x} \cong U_{i+1,j} - U_{i-1,j} / 2h, \quad (20)$$

$$\frac{\partial U}{\partial t} \cong U_{i,j+1} - U_{i,j-1} / 2k. \quad (21)$$

These approximations have errors of order h^2 for x differentiation, and k^2 for t differentiation (for a thorough discussion see ref 44).

Similar approximation schemes for electric field strength, trapped charge density, and free charge density

are:

$$\frac{\partial E^*(x^*, t^*)}{\partial t^*} = E^*_{i, j+1} - E^*_{i, j} / k \quad (22)$$

$$\frac{\partial E^*(x^*, t^*)}{\partial x^*} = E^*_{i, j} - E^*_{i-1, j} / h \quad (23)$$

$$\frac{\partial \rho_t^*(x^*, t^*)}{\partial t^*} = \rho_t^*_{i, j+1} - \rho_t^*_{i, j} / k \quad (24)$$

$$\frac{\partial \rho_f^*(x^*, t^*)}{\partial t^*} = \rho_f^*_{i, j+1} - \rho_f^*_{i, j} / k \quad (25)$$

Before writing the Lax-Wendroff (ref 44) explicit method for the set of equations (8-10) using equations (22-25), we have to find the k/h ratio by some means, in order to get stable solutions.

As we shall see equations (8-10) make a system of hyperbolic partial differential equations of first order, and the condition under which this particular set of partial differential equations has a stable and converging solution is the Courant-Friedrichs-Lowy condition (ref 44).

2.7 Characteristics and hyperbolic equations

A characteristic is a curve in the $(x-t)$ plane along which the integration of a partial differential equation transforms to the integration of an ordinary differential equation. For example if we have

$$a \frac{\partial U}{\partial x} + b \frac{\partial U}{\partial t} = c,$$

where a, b and c are in general a function of x and t and U but not of $\frac{\partial U}{\partial x}$ and $\frac{\partial U}{\partial t}$ then the characteristic curve for this equation is (ref 44)

$$dx/a = dy/b = dU/c,$$

and the equation for the characteristic is simply

$$\frac{dy}{dx} = b/a,$$

and the differential equation for the solution along a characteristic is either

$$adU = cdx \text{ or } bdU = cdy.$$

this means that simply by integrating along this curve we can generate the solution with a particular set of initial and boundary conditions. Then we may ask why bother using finite difference method for a solution? The answer is that programming of the method of characteristics, especially for problems involving a set of simultaneous first order equations, such as equations (8-10), is much more difficult than the programming of the finite difference method. But knowing the characteristics is one way of finding the k/h ratio (The Courant - Friedrich - Lewy condition).

2.8 The Courant-Friedrich-Lowy (C.F.L) condition

Assume that a first order hyperbolic differential equation has been approximated by a difference equation of the form

$$U_{i,j+1} = aU_{i-1,j} + bU_{i,j} + cU_{i+1,j}$$

then U_P (Fig.2.2) depends on the values of U at mesh points A, B, and C. Assume now that the characteristic curve through P of the hyperbolic equation meets the line AC at D and consider AC as an initial line segment. If the initial values along AC are altered then the solution value at P of

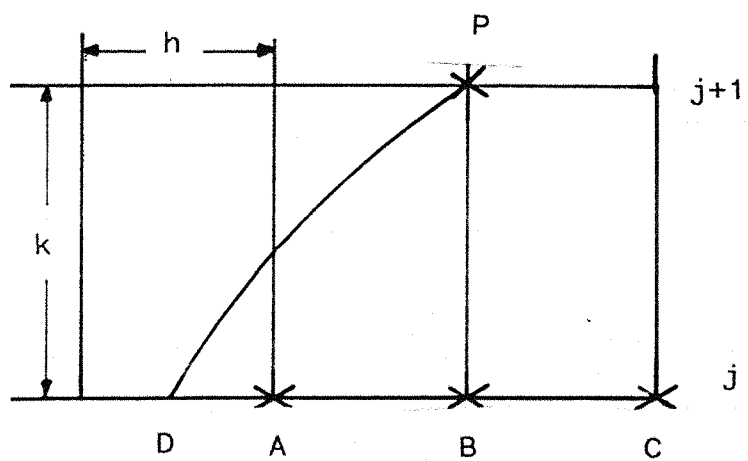


Fig. 2.2: C.F.L condition for first order equations.

[After G.D.Smith ref. 44].

the finite difference equation will change, but these alterations will not affect the solution value at P of the differential equation which depends on the initial value at D. In this case U_P cannot converge to u_P (the solution along characteristic) as $h \rightarrow 0$ and $k \rightarrow 0$. For convergence D must lie between A and C (The Courant-Friedrichs-Lowy condition) i.e the slope of the characteristic curve must be bigger or equal to k/h , which is the condition for convergence.

2.9 Finding the characteristics for equations(8-10)

Recalling the equations

$$\left\{ \begin{array}{l} \rho_f^*(x^*, t^*) E^*(x^*, t^*) + \partial E^*(x^*, t^*) / \partial t^* = 0, \end{array} \right. \quad (8)$$

$$\left\{ \begin{array}{l} \partial E^*(x^*, t^*) / \partial x^* = \rho_f^*(x^*, t^*) + \rho_t^*(x^*, t^*), \end{array} \right. \quad (9)$$

$$\left\{ \begin{array}{l} \partial \rho_t^*(x^*, t^*) / \partial t^* = \rho_f^*(x^*, t^*) / T_f^* - \rho_t^*(x^*, t^*) / T_t^*. \end{array} \right. \quad (10)$$

Eliminating $\rho_f^*(x^*, t^*)$ and defining α and β by

$$\alpha = (1+T_t^* / T_f^*), \text{ and } \beta = (1+T_f^* / T_t^*).$$

and abbreviating $E^*(x^*, t^*)$ to E^* and $\rho_t^*(x^*, t^*)$ to ρ_t^* we

have

$$\left\{ \begin{array}{l} \partial E^* / \partial x^* - T_f^* \partial \rho_f^* / \partial t^* - \beta \rho_t^* = 0, \end{array} \right. \quad (26)$$

$$\left\{ \begin{array}{l} \alpha \partial E^* / \partial t^* + E^* \partial E^* / \partial x^* + T_t^* E^* \partial \rho_t^* / \partial t^* = 0. \end{array} \right. \quad (27)$$

Now if we have a system of simultaneous equations

$$\left\{ \begin{array}{l} a_1 \partial U / \partial x + b_1 \partial U / \partial y + c_1 \partial V / \partial x + d_1 \partial V / \partial y + e_1 = 0, \quad (28) \\ \\ a_2 \partial U / \partial x + b_2 \partial U / \partial y + c_2 \partial V / \partial x + d_2 \partial V / \partial y + e_2 = 0, \quad (29) \end{array} \right.$$

It can be shown (ref 44) that equations (28-29) have characteristics given by

$$(a_1 c_2 - a_2 c_1) (dy/dx)^2 - (a_1 d_2 - a_2 d_1 + b_1 c_2 - b_2 c_1) dy/dx + (b_1 d_2 - b_2 d_1) = 0. \quad (30)$$

Here, if we have two real and distinct roots then the simultaneous system of partial differential equations (28-29) are called *hyperbolic*, and if one real root then they are called *parabolic*, and if no real root at all they are called *elliptic*.

If we take $E^* = U$, $\rho_t^* = V$, $x^* = y$ and $t^* = y$, then equation (30) is

$$\alpha T_f^* (dx^* / dt^*)^2 - (E^* T_t^* + E^* T_f^*) (dx^* / dt^*) = 0, \quad (31)$$

which has roots

$$dx^* / dt^* = 0, \text{ and } dx^* / dt^* = E^*.$$

Correspondingly, the system of equations (8-10) is *hyperbolic*. Now in the (x^*, t^*) plane the slopes at the characteristics have the forms

$$dt^* / dx^* = \infty \quad (32) \quad \text{and} \quad dt^* / dx^* = 1 / E^*. \quad (33)$$

This means that for a solution corresponding to (32) and $x^* = 0$, the characteristic does not leave x^* axis. Applying the C.F.L. condition we have $k/h \leq \infty$, which is a trivial condition

and for (33), $k/h \leq 1/E^*$; with the biggest value for E^* (unity) the condition is simply $h \leq k$.

So if we choose the condition $k=h$, then for smaller values of E^* , we will have $k \leq h$, which means that the solutions are always converging and stable.

2.10 Solution of the reduced partial differential equations(8-10)

Since the ratio, k/h is now known it is possible to use the approximation derivatives (22-25) in (8-10), and find the explicit solution. Putting (22-25) in (8-10) and solving the resultant equations for ρ_t^* , ρ_f^* and E^* yields

$$\left\{ \rho_t^*_{i,j+1} = (E^*_{i,j} - E^*_{i-1,j})k/(hT_f^*) + \rho_t^*_{i,j}(1-\beta k/T_f^*), \quad (34) \right.$$

$$\left\{ \rho_f^*_{i,j} = (E^*_{i,j} - E^*_{i-1,j})/h - \rho_t^*_{i,j}, \quad (35) \right.$$

$$\left. \left\{ E^*_{i,j+1} = E^*_{i,j} - k\rho_f^*_{i,j}E^*_{i,j}. \quad (36) \right. \right.$$

Equations (34-36) are explicit Lax-Wendroff schemes (ref 44) for the set of equations(8-10).

If we divide the x^* axis into n equal segments and the t^* axis into m equal segments, with $0 \leq x^* \leq 1$ and for special case of times up to transit time (i.e $0 \leq t^* \leq 1$), we have

$$h = 1/n, \quad \text{and} \quad k = 1/m.$$

Since $k \leq h$, the condition as the mesh points in the $(x^* - t^*)$ plane is

$$m \geq n$$

$$(37)$$

To extend the solution to times longer than the transit time (unity for the reduced model), we simply have to increase time divisions. For example $m=40$, and $n=20$ would be the right number of mesh points for times up to twice the transit time.

2.11 Calculation of the surface potential

Once the distribution of the electric field in the sample is known, then it is possible to find the surface potential variation, via equation (11). The integration is most conveniently done by Simpson's rule to sufficient accuracy.

$$\int_a^b f(x)dx \approx h/3[f(a)+4f(x_1)+f(b)]$$

where $h=(a-b)/2$ and x_1 is the midpoint between a and b i.e. $(a+b)/2$.

This method is unsuitable for use over a large interval, so a piecewise technique must be used. In this technique $(a-b)$ is divided into $2m$ equal strips of width h , where m is an integer.

Using the above approximation we have:

$$\int_a^b f(x)dx = h/3[f(a)+2\sum_{i=1}^{m-1} f(x_{2i})+4\sum_{i=1}^m f(x_{2i-1})+f(b)]$$

where $a=x_0 < x_1 < x_2 \dots < x_{2m} = b$, $h=(b-a)/2m$, and $x_i = x_0 + ih$ for each $i=0, 1, \dots, 2m$ (ref. 47).

In our particular case, the x^* axis is divided into 20 segments ($0 \leq x^* \leq 1$), hence $m=10$, $a=0$, $b=1$, and $h=1/20$. So for an arbitrary time t_1 we have

$$V^*(t_1) = \int_0^1 E^*(x^*, t^*) dx^* \cong 1/60 (E^*_{0,t_1} + E^*_{1,t_1} + 4E^*_{0.05,t_1} + 2E^*_{0.1,t_1} + 4E^*_{0.15,t_1} + \dots + 2E^*_{0.9,t_1} + 4E^*_{0.95,t_1}). \quad (38)$$

2.12 Programming of the explicit Lax-Wendroff schemes(34-36)

Recalling the boundary and initial conditions(12-15)

$$\rho_f^*(x^*, 0) = \gamma \delta(x^*), \quad \text{for } 0 \leq x^* \leq 1 \text{ and } 0 \leq \gamma \leq 1 \quad (12)$$

$$E^*(x^*, 0) = 1, \quad \text{for } 0 < x^* \leq 1 \quad (13)$$

$$E^*(0, t^*) = 1 - \gamma, \quad (14)$$

$$\rho_t^*(x^*, 0) = 0. \quad \text{for } 0 \leq x^* \leq 1 \quad (15)$$

And since we have only three Lax-Wendroff schemes(34-36), we need only three boundary conditions. As we shall see equation (12) is superfluous since it is generated by the calculation. Writing equations(13-15) using subscript notations

$$E_{i,0}^* = 1, \quad \text{for } i=1 \text{ to } i=n \quad (i \text{ being an integer}) \quad (39)$$

$$E_{0,j}^* = 1 - \gamma, \quad \text{for } j=0 \text{ to } j=m \quad (j \text{ being an integer}) \quad (40)$$

$$\rho_{t,i,0}^* = 0. \quad \text{for } j=0 \text{ to } j=m. \quad (41)$$

The programming was implemented in BASIC on ApricotTM micro

computer during the early stages of development and later transferred to an IBMTM AT micro computer for larger addressable memory using the MicrosoftTM c.5 Optimizing Compiler. The C language was used for its speed and compactness of code.

For practical considerations the number of mesh points chosen are $n=20$ and $m=600$, to give times up to 30 transit times.

The central body of the programme is essentially two nested DO loops for i and j , within which the electric field, trapped charge density and free charge density are calculated. A second routine performs the integration of the electric field using Simpson's rule (38), to yield the time variation of the surface potential.

CHAPTER 3 : RESULTS AND DISCUSSION

3.1 Results

3.1.1 Experimental results

Samples of polyethylene film of 30 micro meters thickness were held on an earthed metal backing electrode on a turntable, and subsequently positively charged using a corona discharge unit.

Immediately after the cessation of charging successive decay measurements were taken, using an electrostatic probe, rotating the turntable below the probe. The time variation of surface potential was monitored using an X-Y point recorder. The first decay curve was recorded for films charged to the lowest voltage to be used. Then the charging voltage was increased and again the decay was recorded. This procedure was repeated 5 times altogether, and 30 minutes were allowed between each run. The decay profiles are shown in Fig 3.1.

3.1.2 Curve fitting technique

Once the solutions to the reduced model are found, it is possible to find the values for $\rho_f(x,t)$, $\rho_t(x,t)$, $E(x,t)$ and $V(t)$, provided that γ , T_f , T_t , and μ are known. Recall that these parameters are related to the reduced values by

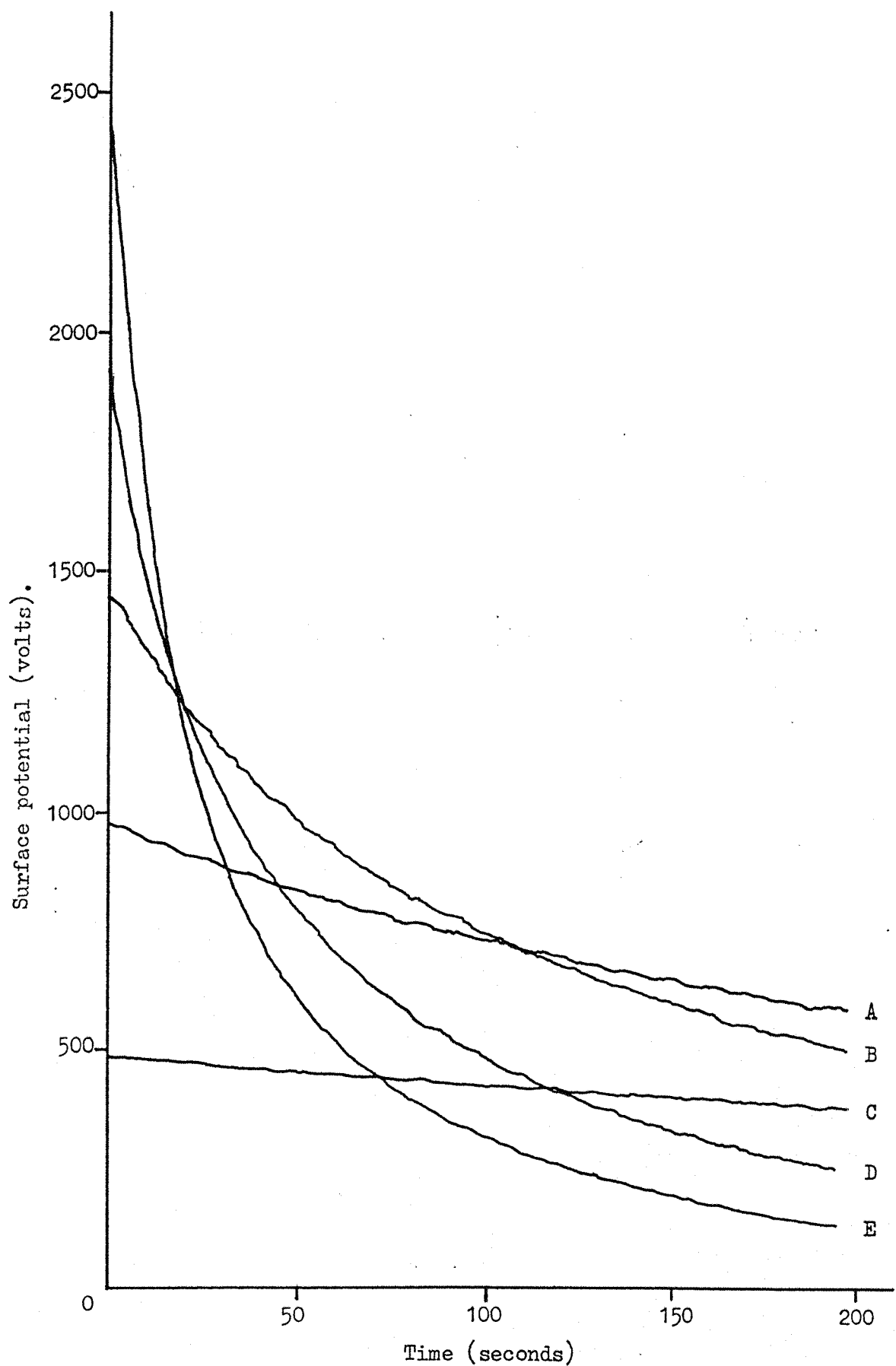


Fig. 3.1: Experimental plots of surface potential versus time showing crossover phenomenon. A, 975 volts; B, 1462 volts; C, 492 volts; D, 2000 volts; and E, 2500 volts. Sample thickness=30 μ m.

$$\begin{aligned}
 x &= x^* L, \quad t = t^* t_0, \quad T_f = T_f^* t_0, \quad T_t = T_t^* t_0 \\
 \rho_f(x, t) &= \rho_f^*(x^*, t^*) v_0 \varepsilon \varepsilon_0 / L^2, \quad \rho_t(x, t) = \rho_t^*(x^*, t^*) v_0 \varepsilon \varepsilon_0 / L^2, \\
 E(x, t) &= E^*(x^*, t^*) v_0 / L, \quad V(t) = V^*(t^*) v_0 \\
 \mu &= L^2 / (t_0 v_0).
 \end{aligned}$$

In order to determine the four parameters we must resort to curve fitting techniques. One way of utilising this method is to use a function to fit the theoretical $V(t)$ curve to the experimental data. As yet there is no function available to fit the four parameters to the experimental curves; so another method based on randomly generated numbers was used.

In this method, four independent randomly generated numbers are produced and then weighted properly by some factor, in order to bring the search into a quicker conclusion. The run time library routine `rand()` function of the Microsoft C compiler, which generates a random integer in the range 0-32767, performed the task.

The five different experimental data sets $V(t)$ were each sampled every 10 seconds and the resultant voltages were stored as an array of integers in a version of the programme developed to perform the curve fitting. Since there are 600 time intervals for the theoretical $V(t)$ corresponding to 200 seconds of experimental data, there is one theoretical point corresponding to every experimental point and therefore there is no need to perform any interpolations. When a theoretical voltage profile is produced using the randomly generated numbers, a comparison is made with the experimental results. The chi square statistic is used as a test of "goodness of

fit". After each random trial χ^2 is calculated and if it is found to be much larger than the number of experimental points a new set of numbers are generated and another value of the χ^2 value is found. This process is reiterated , until a good fit is found. χ^2 can be calculated using (ref 48)

$$\chi^2 = \sum \frac{(\text{observed} - \text{expected})^2}{\text{variance}}$$

where "observed" is the experimental value of voltage, and "expected" is the theoretical values.

Errors for these particular experiments were assessed to be ± 10 volts.

A programme function named "chi_square" was developed to calculate each χ^2 value for a particular set of transport parameters.

3.1.3 Evaluation of the transport parameters

For the 2500 voltage profile, the programme was set to reject values of χ^2 bigger than 700. Then the computer was left to run overnight to accumulate sets of parameters with χ^2 smaller than 700. Then by making a systematic search i.e. changing the value of one parameters slightly while keeping the rest constant, it was possible to reduce χ^2 significantly.

This procedure was repeated for the 2000 and 1462 voltage profiles. For the 975 and 492 voltage profiles the programme

was set to reject χ^2 values bigger than 100 and, again by systematically searching, the χ^2 values were further reduced. Table 1 shows the best fit transport parameters, from which the corresponding $V(t)$ (Fig. 3.2-3.6), $E(x,t)$, $\rho_f(x,t)$, $\rho_t(x,t)$ and total charge in the sample (i.e. $\rho_{tot}(t)$) can be plotted using the graphic facilities of LotusTM 1 2 3.

3.1.4 The von Berlepsch model

Based on the transport equations (1-6) von Berlepsch (ref 25) has derived an analytical approximation to $V(t)$. The solution which has a time range up to the transit time t_0 , is given by:

$$V(t) = V_0 - \mu (V_0/4L)^2 [1 - (1-\gamma)^2] \frac{1}{R} \frac{[rt + \omega(1 - \exp(-R/t))]}{R} \quad (42)$$

where

t is the time, $r = 1/T_t$, $\omega = 1/T_f$, $R = r + \omega$ and V_0 is the initial surface potential.

Using the parameters of table 1 and equation (42) a set of voltage decay graphs was produced for comparison with the numerical model. It should be noted that these parameters may not correspond to the best fit of the von Berlepsch model, nevertheless it is clear that there are significant differences between the two models (Fig. 3.7).

Initial surface potential(volts)	2500	2000	1462	975	492
Initial electric field (MV/m)	83.3	66.67	48.7	32.5	16.4
γ	1	0.9455	0.693	0.500	0.255
T_f (seconds)	8.72	22.80	79.44	372.6	1232.8
T_t (seconds)	6.21	17.70	25.83	1408.8	5424.5
μ ($m^2 V^{-1} s^{-1}$) $\times 10^{-14}$	2.576	1.845	0.929	0.683	1.095
transit time (seconds)	13.9	24.3	64.5	131.6	164.3
χ^2	69.38	59.84	59.79	7.02	0.964

Table 1. Different transport parameters derived from the curve fittings. Sample thickness $30\mu m$.

2500 volts

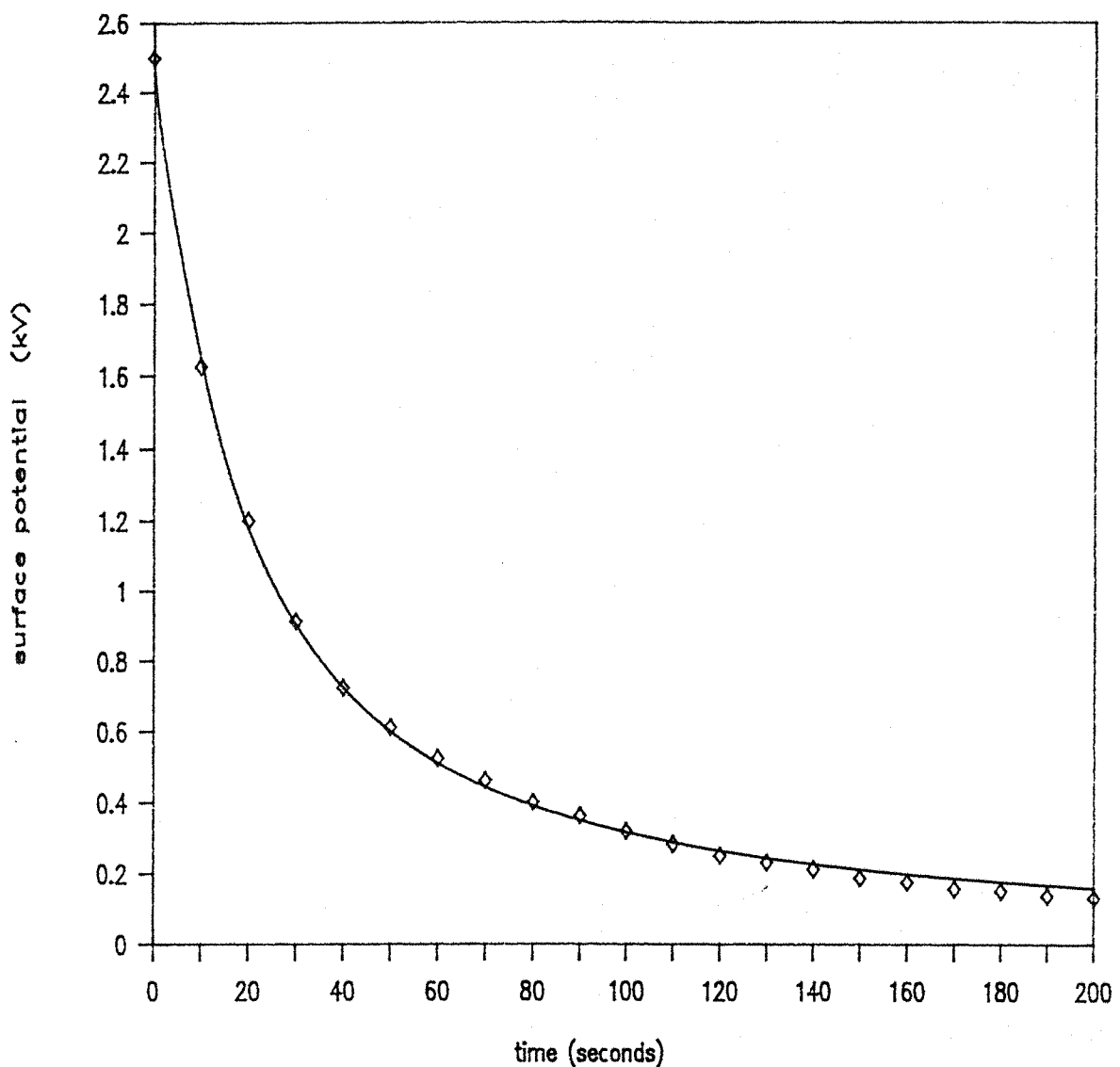


Fig. 3.2 : Surface potential decay

◇ experimental values,

— theoretical values.

$$\gamma = 1, T_f = 8.72 \text{ sec}, T_t = 6.21 \text{ sec}, \mu = 2.576 \times 10^{-14} \text{ m}^2 \text{ V}^{-1} \text{ s}^{-1}$$

2000 volts

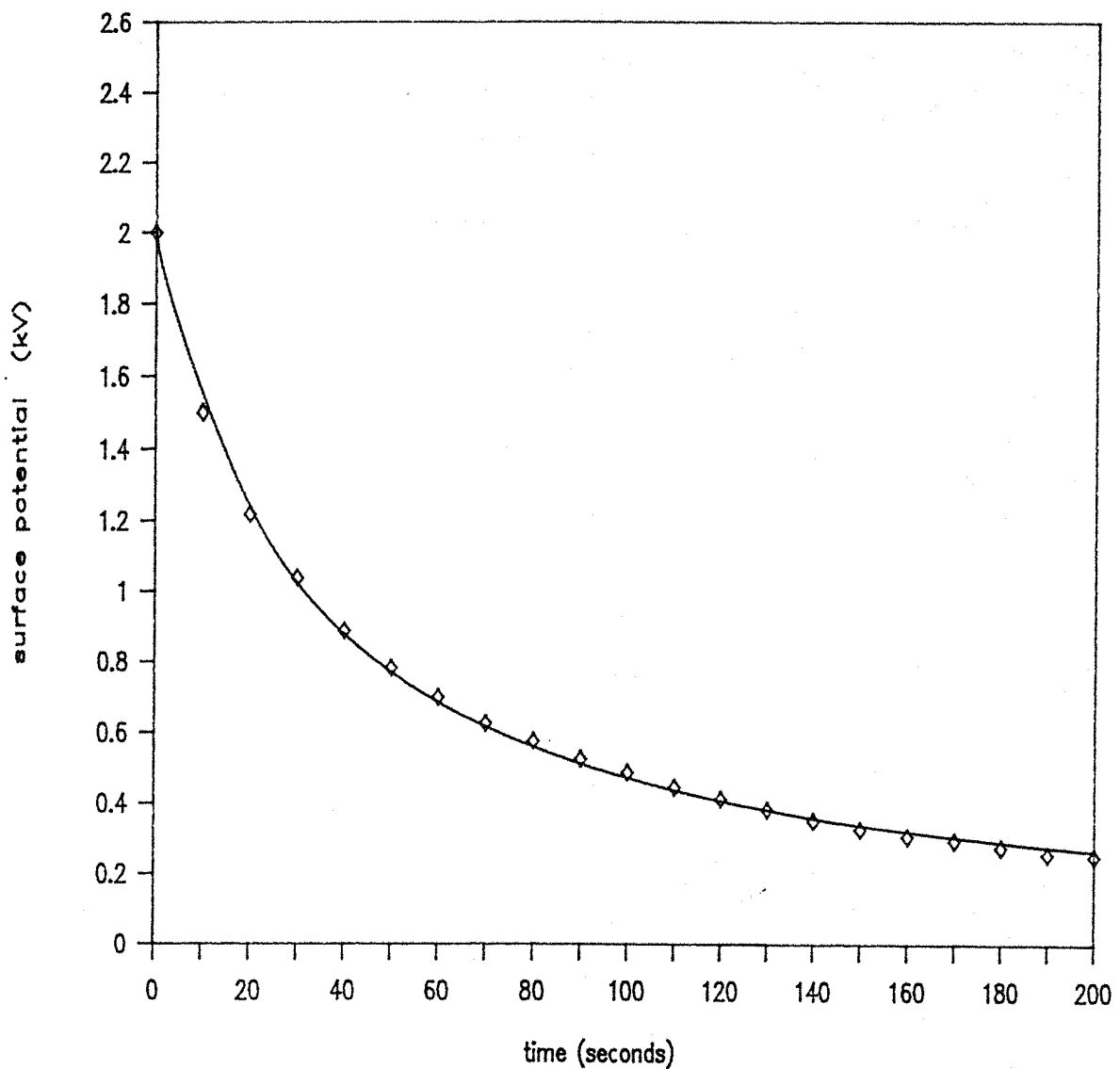


Fig. 3.3 : Surface potential decay

◇ experimental values,

— theoretical values.

$$\gamma = 0.9455, T_f = 22.80 \text{ sec}, T_t = 17.70 \text{ sec}, \mu = 1.845 \times 10^{-14} \text{ m}^2 \text{ V}^{-1} \text{ s}^{-1}.$$

1462 volts

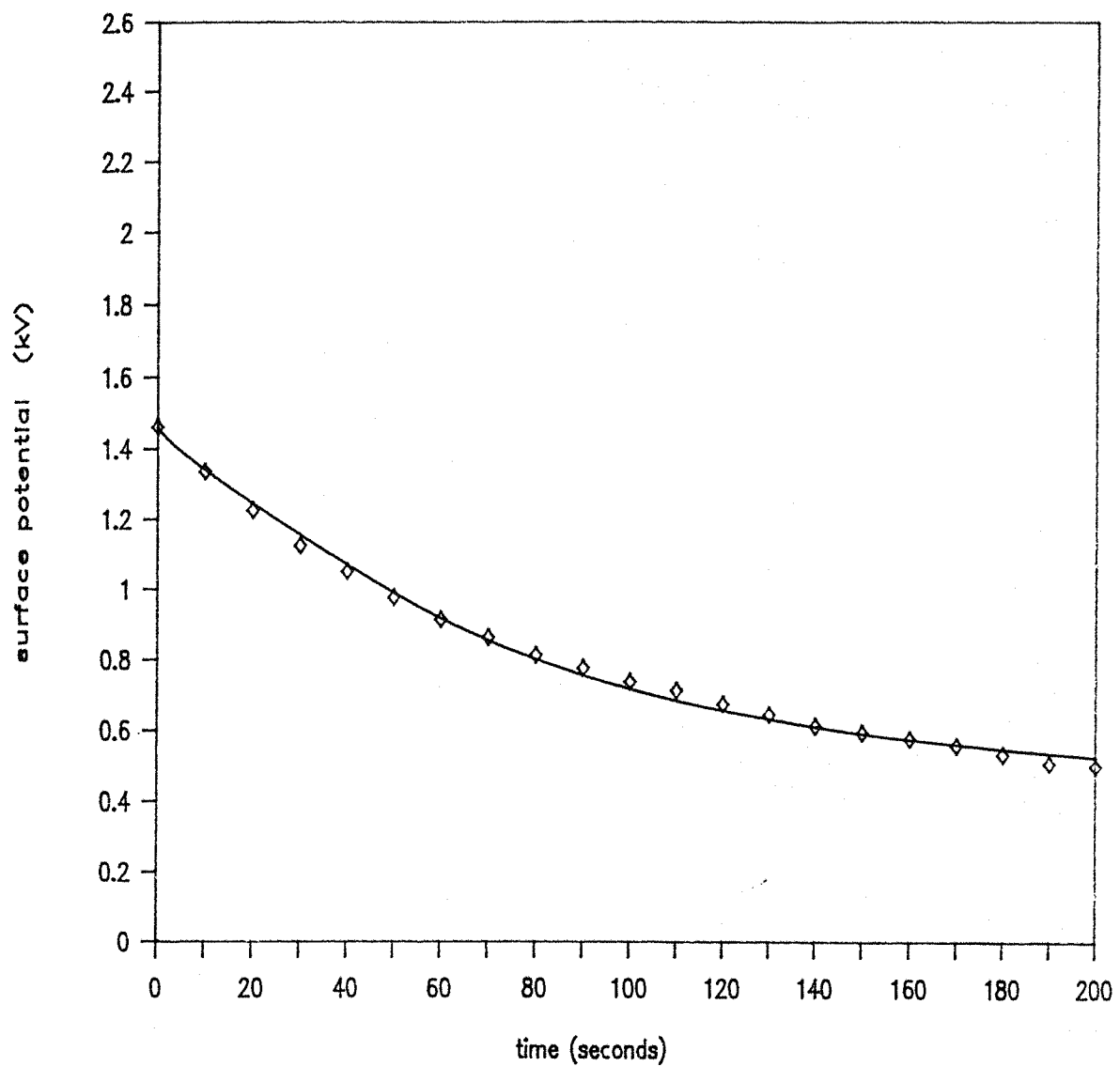


Fig. 3.4 : Surface potential decay

◇ experimental values,

— theoretical values.

$$\gamma = 0.693, T_f = 79.44 \text{ sec}, T_t = 25.83 \text{ sec}, \mu = 9.29 \times 10^{-15} \text{ m}^2 \text{ V}^{-1} \text{ s}^{-1}.$$

975 volts

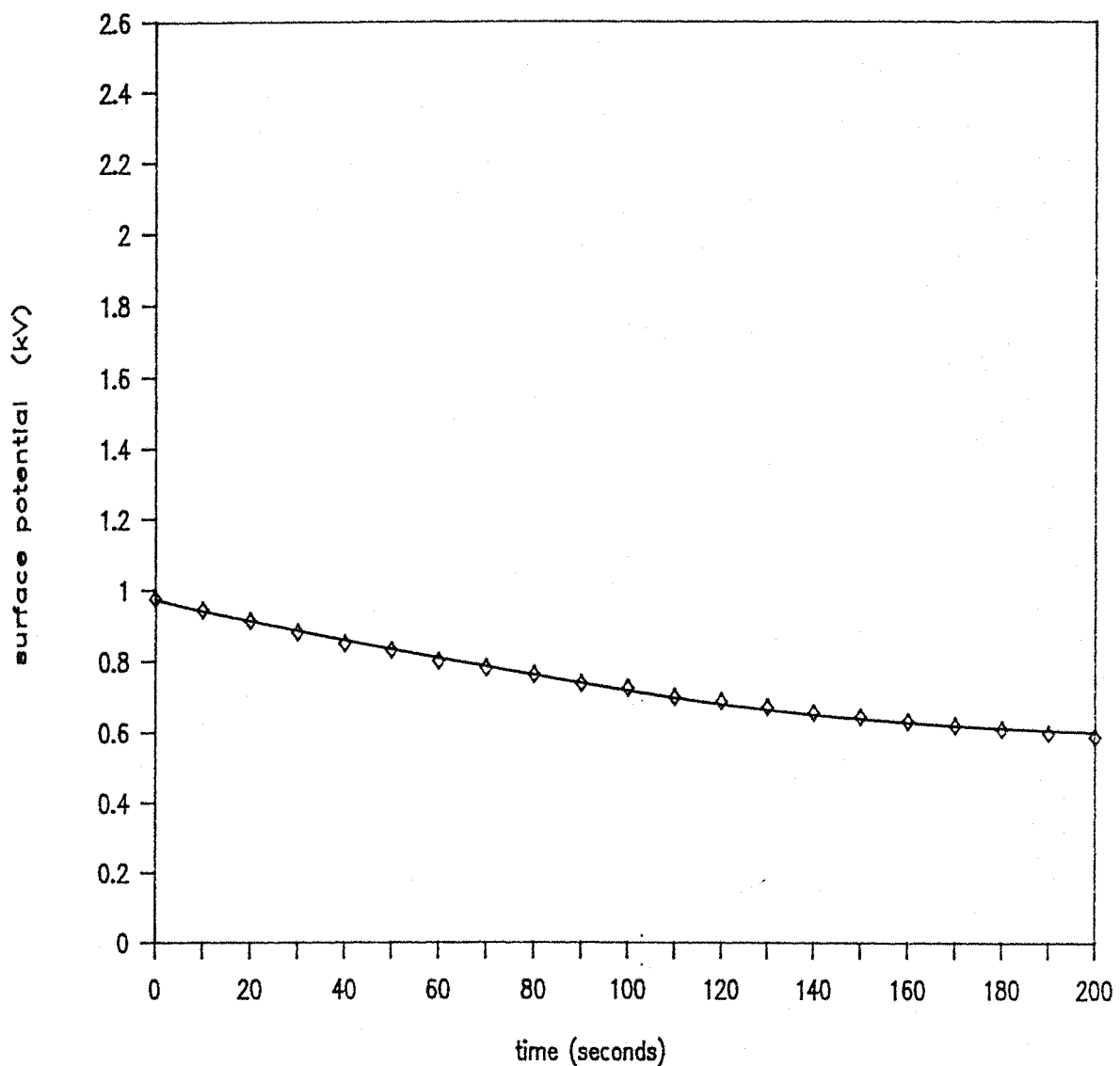


Fig. 3.5 : Surface potential decay

◇ experimental values,

— theoretical values.

$$\gamma = 0.500, T_f = 372.6 \text{ sec}, T_t = 1408.8 \text{ sec}, \mu = 6.835 \times 10^{-15} \text{ m}^2 \text{ V}^{-1} \text{ s}^{-1}.$$

492 volts

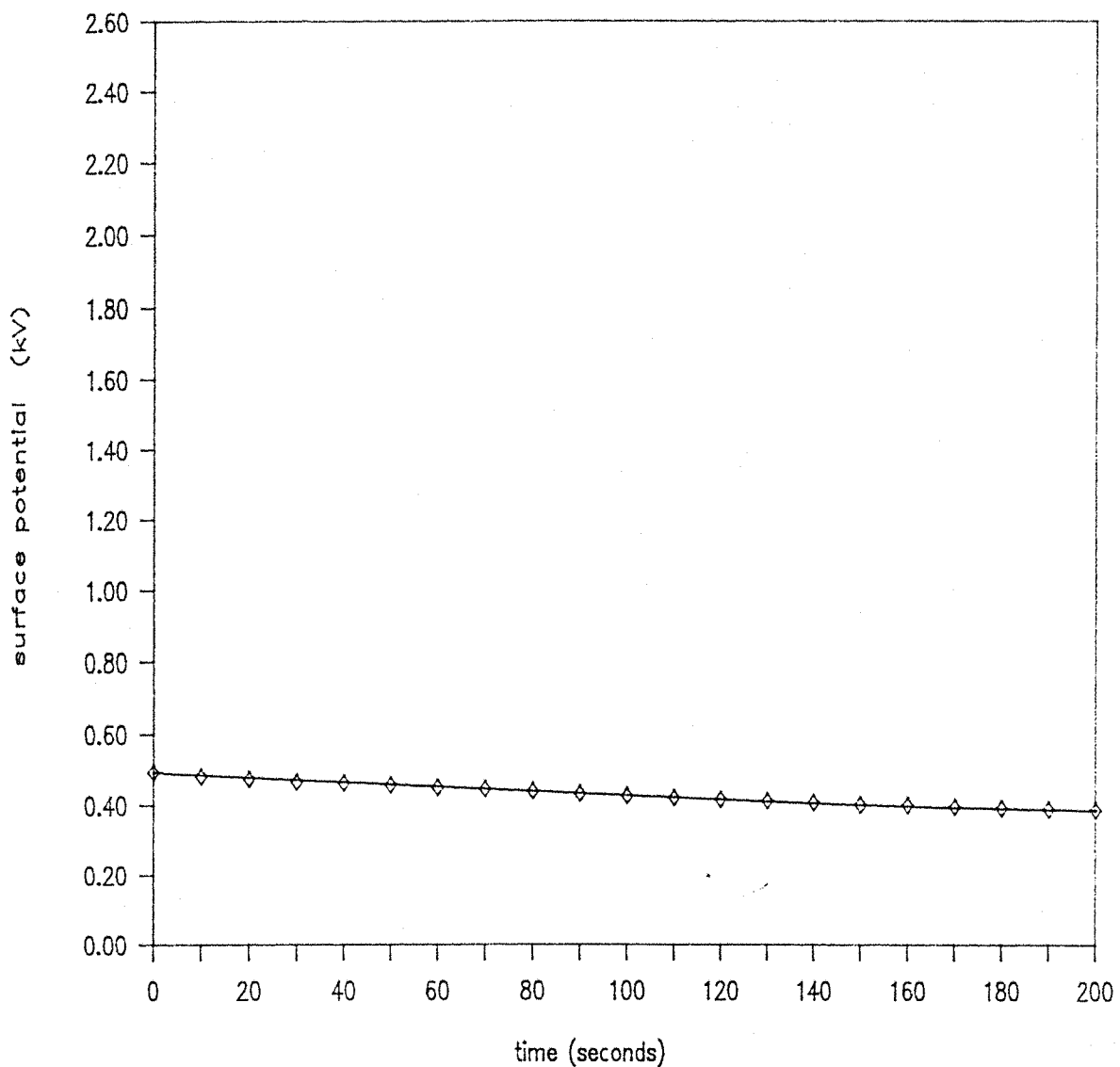


Fig. 3.6 : Surface potential decay

◇ experimental values,

— theoretical values.

$$\gamma = 0.255, T_f = 1232.8 \text{ sec}, T_t = 5424.5 \text{ sec}, \mu = 1.095 \times 10^{-14} \text{ m}^2 \text{ V}^{-1} \text{ s}^{-1}$$

The von Berlepsch model

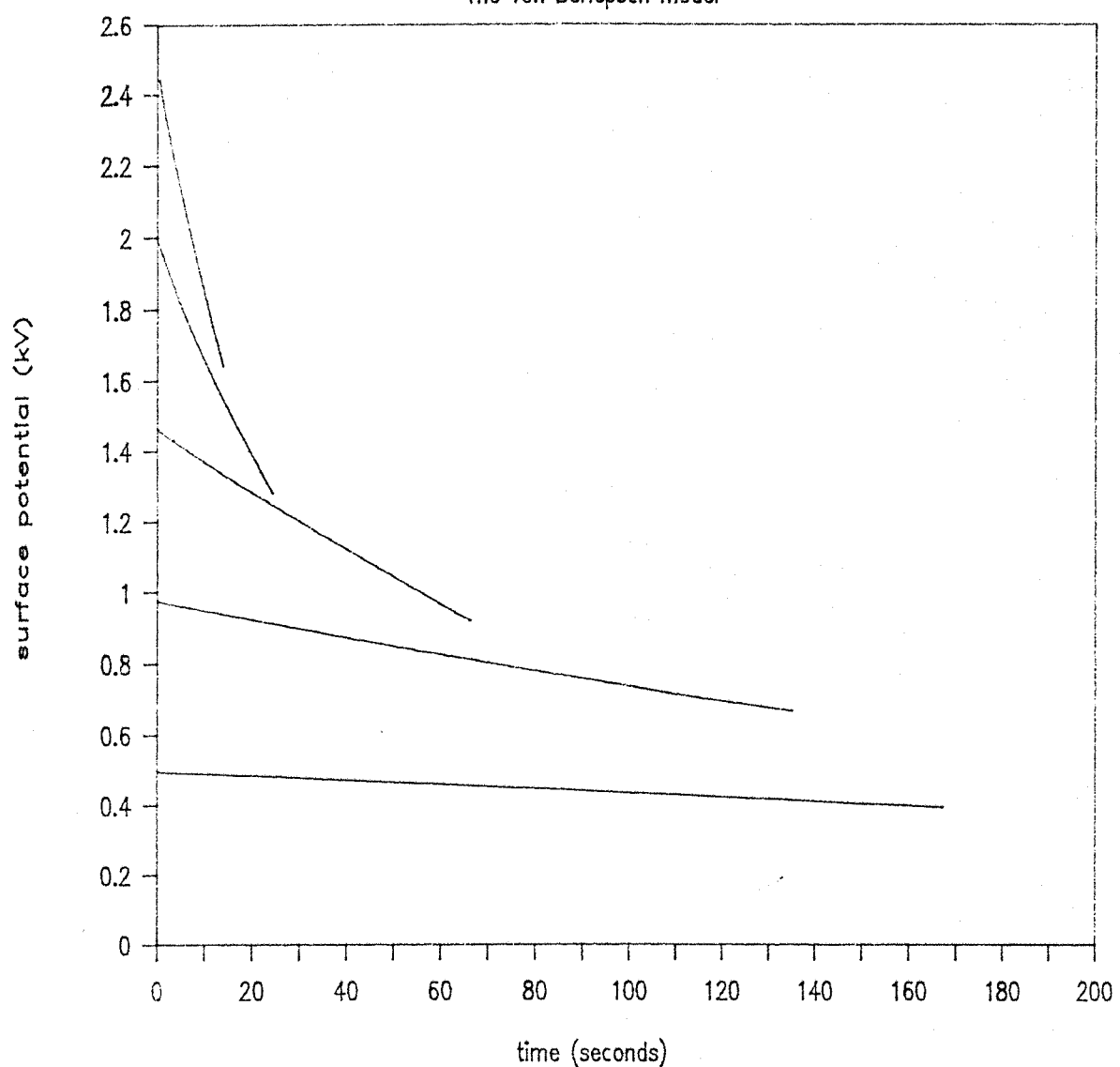


Fig. 3.7: Surface potential decays based on the von Berlepsch model using the parameters of Table 1.

3.2 The derived results

3.2.1 The electric field strength

As expected Fig. 3.8-3.12 show that the electric field is constant across the sample prior to injection of charge. Immediately after injection, the electric field at the surface drops to a level depending on the values of γ and the initial surface potential. As time goes on the electric field at the opposite electrode starts to drop and for times far longer than the duration of the experiment the value of the field at this electrode eventually equals the electric field at the surface, as expected.

3.2.2 The free charge density

Immediately after injection, the free charge density in the sample is very large just inside the sample and, as time increases, the charge begins to spread out in the sample. For cases where $\gamma \neq 1$, the peak of the distribution moves towards the opposite electrode since the free charge is repelled by the remaining charge trapped at the surface. But when $\gamma = 1$, the peak remains at $x=0$ since no charge remains at the surface. As time increases, the peak of the distribution becomes smaller and eventually all the free charge leaves the sample. Fig. 3.13 - 3.17 show the free charge density distributions for different initial surface potentials.

2500 volts

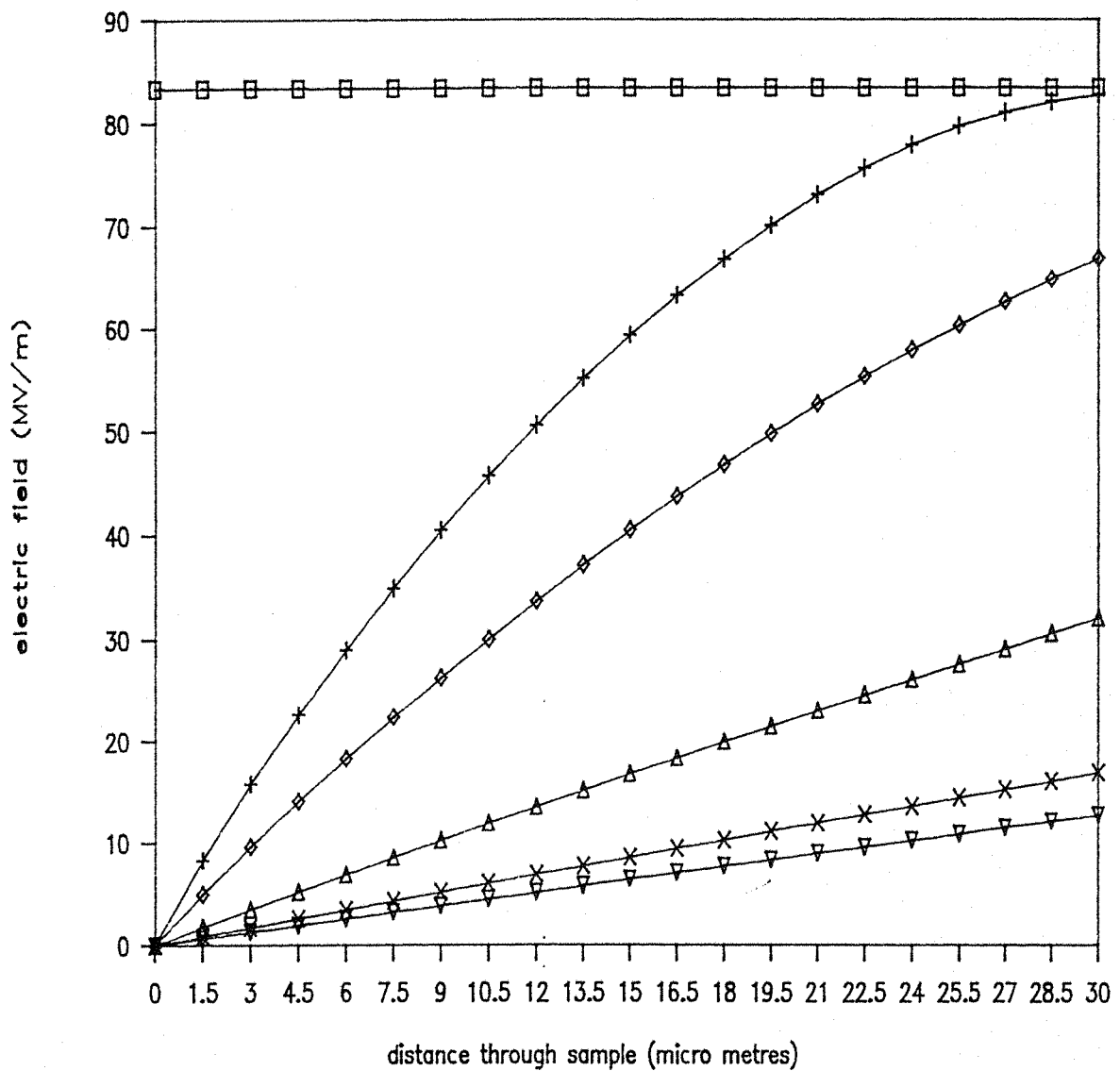


Fig. 3.8 : The electric field distribution through the sample for different times.

- before charge injection,
- + after 10 seconds,
- ◊ after 20 seconds,
- △ after 60 seconds,
- ✗ after 120 seconds,
- ▽ after 160 seconds.

$$\gamma=1, T_f=8.72 \text{ sec}, T_t=6.21 \text{ sec}, \mu=2.576 \times 10^{-14} \text{ m}^2 \text{ V}^{-1} \text{ s}^{-1}.$$

2000 volts

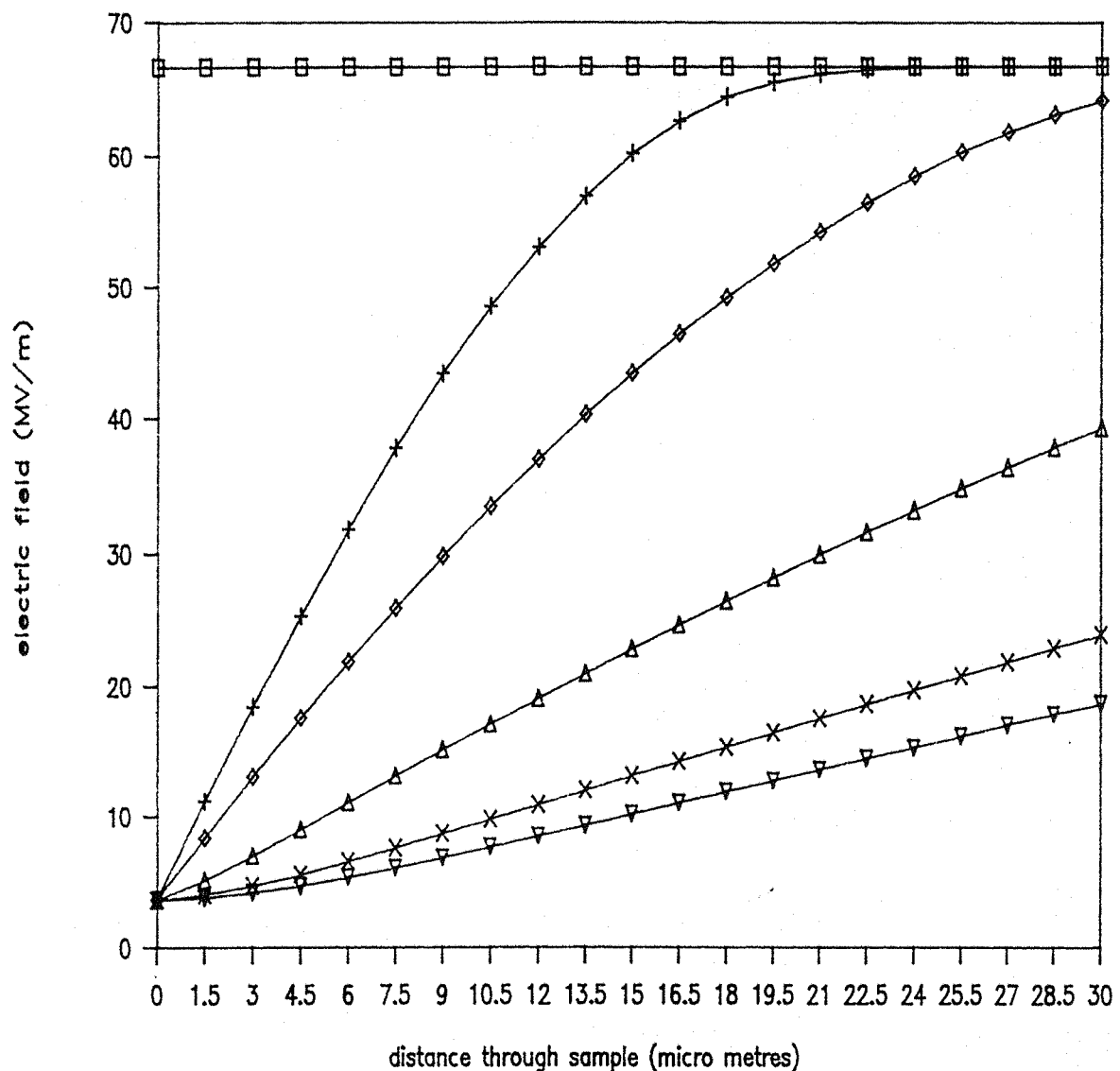


Fig. 3.9 : The electric field distribution through the sample for different times.

- before charge injection,
- + after 10 seconds,
- ◊ after 20 seconds,
- △ after 60 seconds,
- Х after 120 seconds,
- ▽ after 160 seconds.

$$\gamma = 0.9455, T_f = 22.80 \text{ sec}, T_t = 17.70 \text{ sec}, \mu = 1.845 \times 10^{-14} \text{ m}^2 \text{ V}^{-1} \text{ s}^{-1}.$$

1462 volts

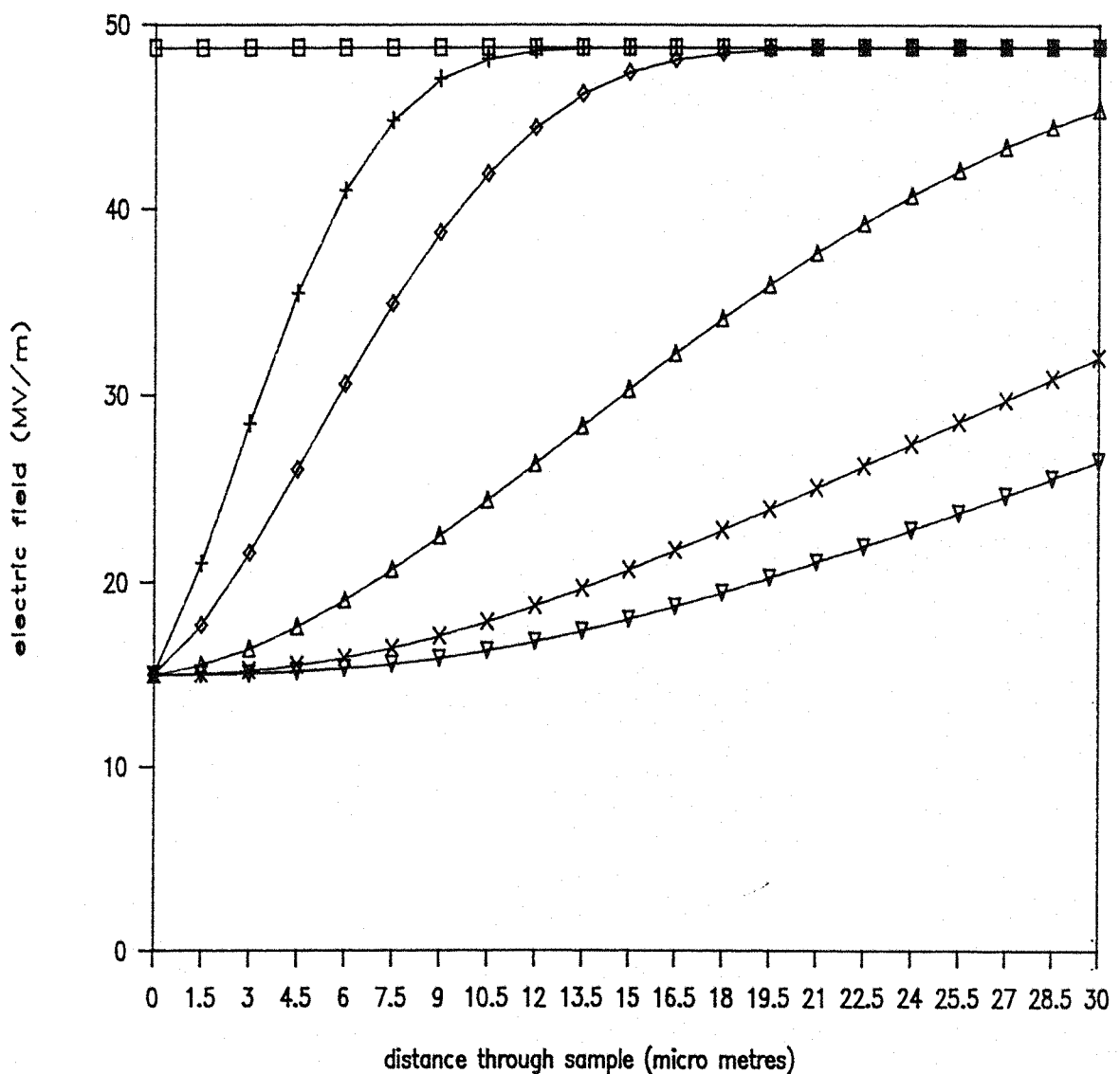


Fig. 3.10 : The electric field distribution through the sample for different times.

- before charge injection,
- + after 10 seconds,
- ◊ after 20 seconds,
- △ after 60 seconds,
- × after 120 seconds,
- ▽ after 160 seconds.

$$\gamma = 0.693, T_f = 79.44 \text{ sec}, T_t = 25.83 \text{ sec}, \mu = 9.29 \times 10^{-15} \text{ m}^2 \text{ V}^{-1} \text{ s}^{-1}.$$

975 volts

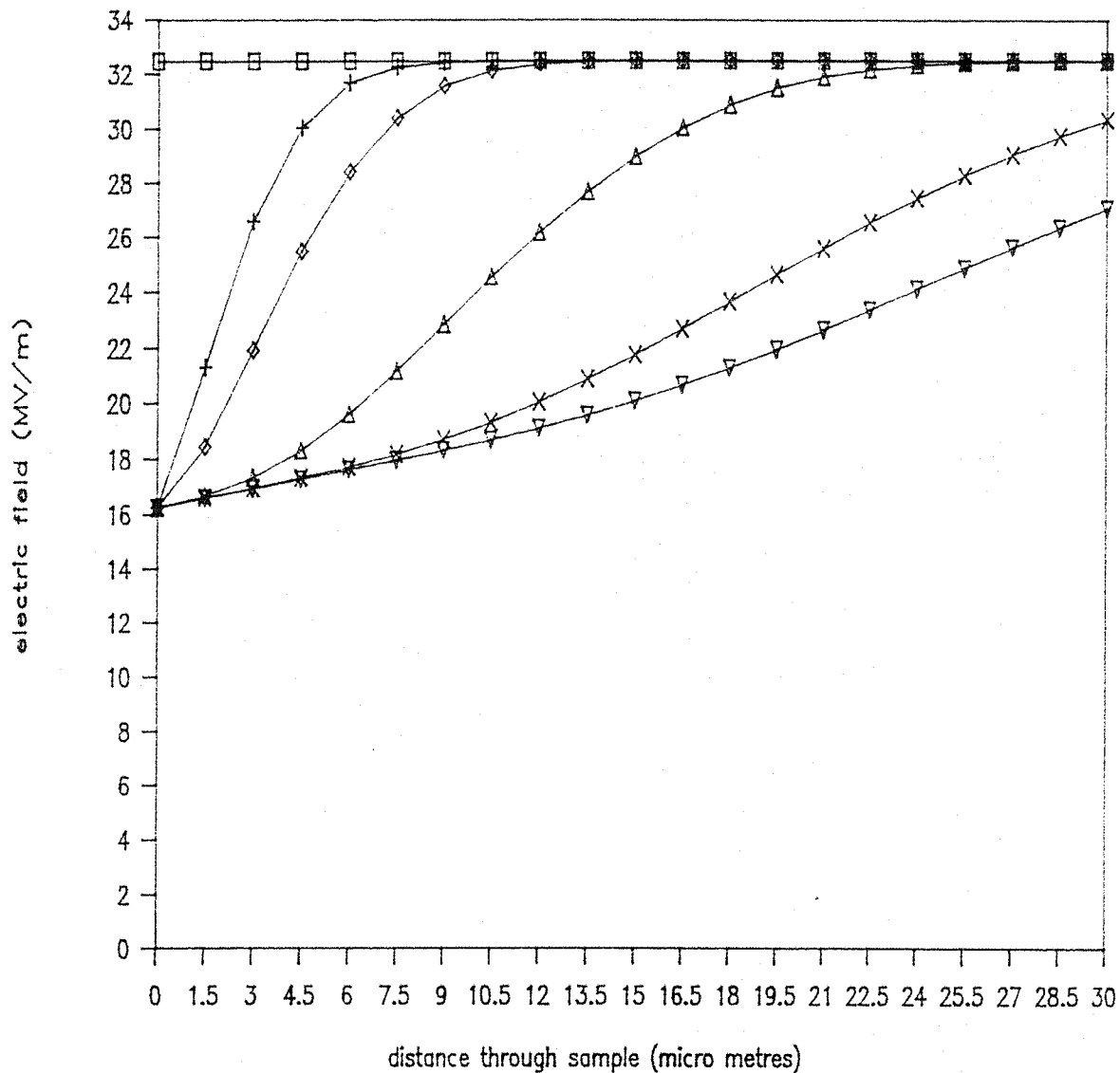


Fig. 3.11 : The electric field distribution through the sample for different times.

- before charge injection,
- ⊕ after 10 seconds,
- ◇ after 20 seconds,
- △ after 60 seconds,
- × after 120 seconds,
- ▽ after 160 seconds.

$$\gamma = 0.500, T_f = 372.6 \text{ sec}, T_t = 1408.8 \text{ sec}, \mu = 6.835 \times 10^{-15} \text{ m}^2 \text{ V}^{-1} \text{ s}^{-1}.$$

492 volts

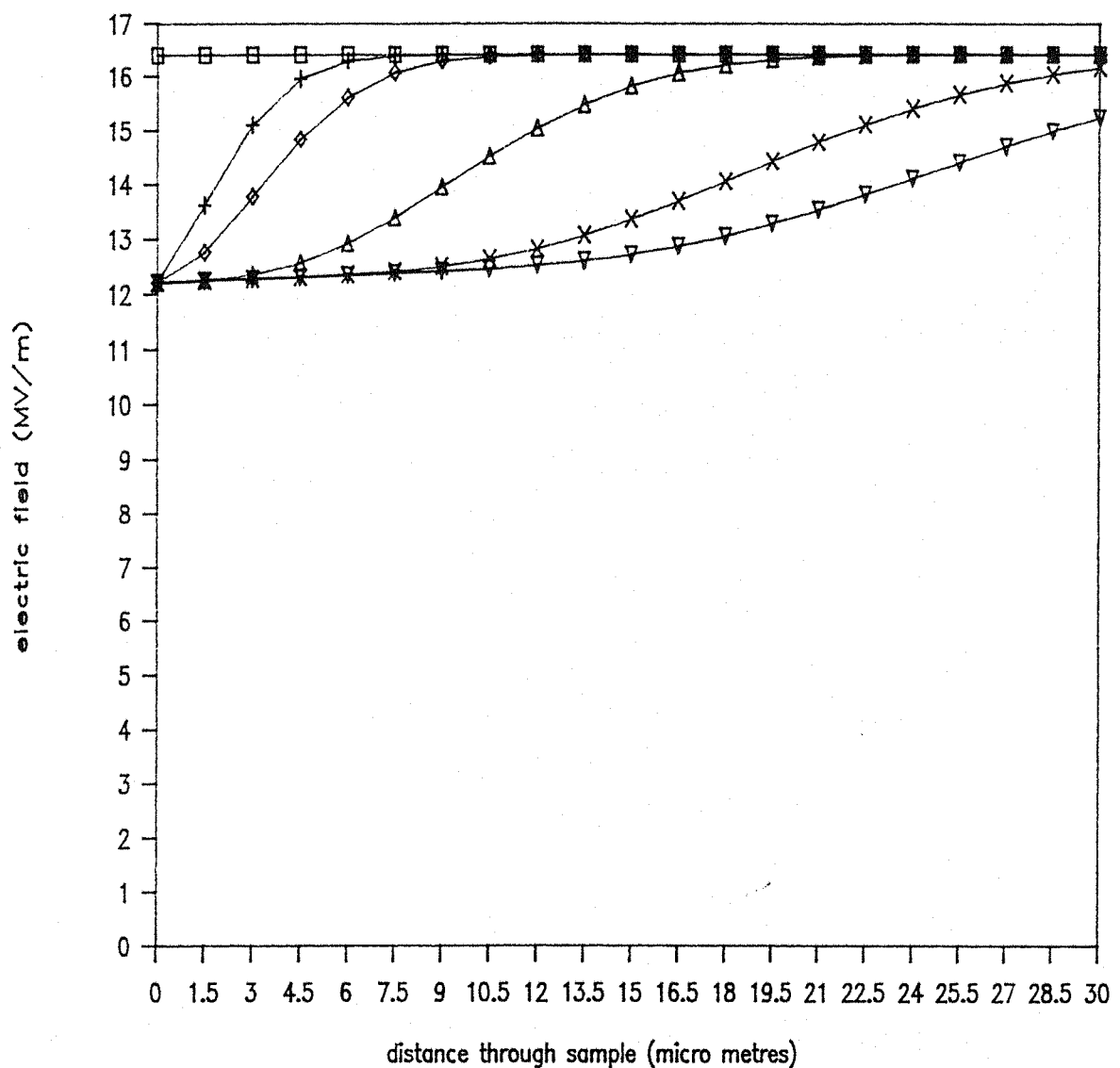


Fig. 3.12 : The electric field distribution through the sample for different times.

- before charge injection,
- ⊕ after 10 seconds,
- ◇ after 20 seconds,
- △ after 60 seconds,
- × after 120 seconds,
- ▽ after 160 seconds.

$$\gamma = 0.255, T_f = 1232.8 \text{ sec}, T_t = 5424.5 \text{ sec}, \mu = 1.095 \times 10^{-14} \text{ m}^2 \text{ V}^{-1} \text{ s}^{-1}$$

2500 volts

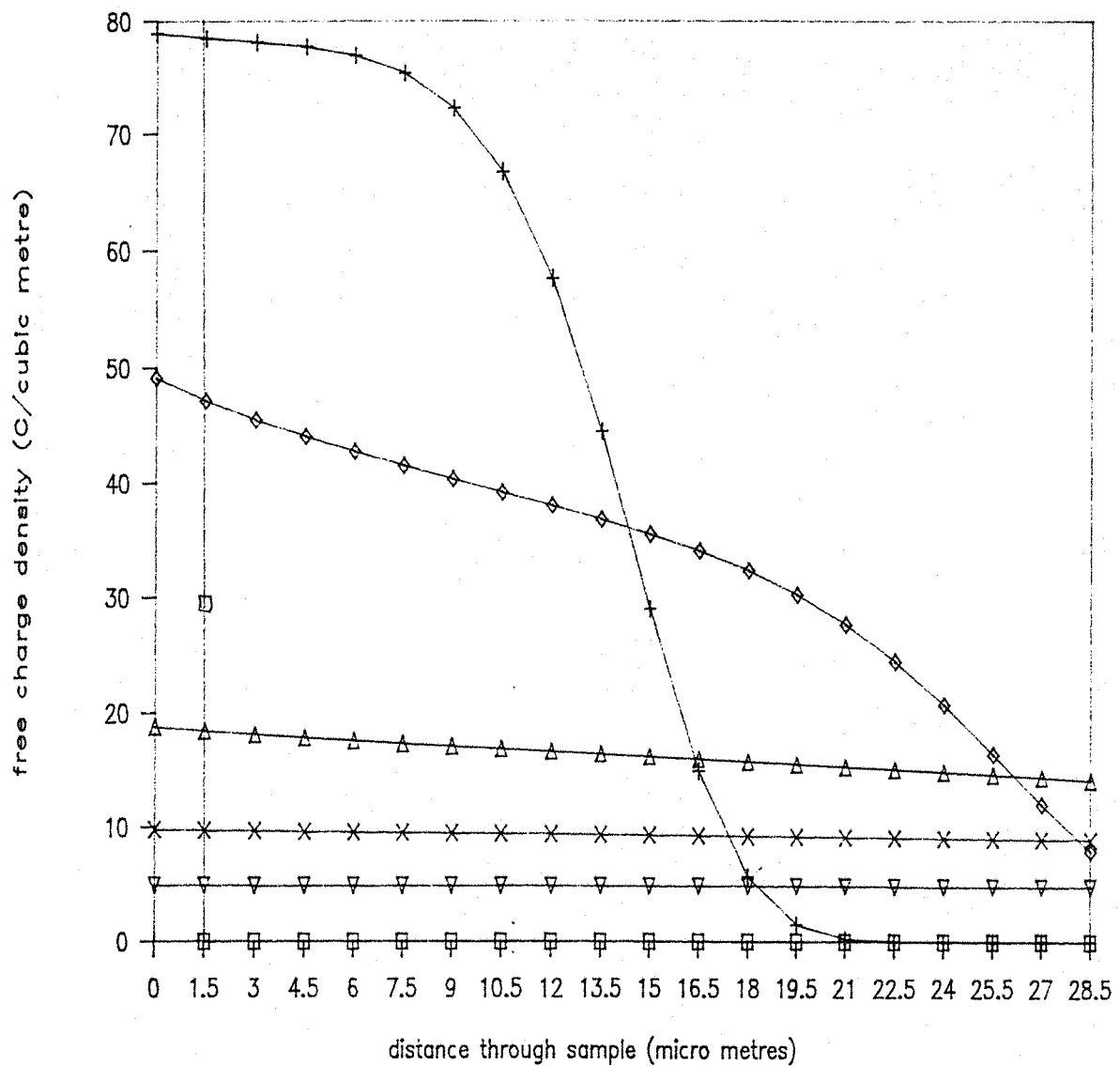


Fig. 3.13 : The free charge density distribution through the sample for different times. $\epsilon\epsilon_0 = 2 \times 10^{-11} \text{ F/m.}$

- at $t=0$ (just after the injection),
- ⊕ after 5 seconds,
- ◇ after 10 seconds,
- △ after 40 seconds,
- × after 80 seconds,
- ▽ after 160 seconds.

$$\gamma = 1, T_f = 8.72 \text{ sec}, T_t = 6.21 \text{ sec}, \mu = 2.576 \times 10^{-14} \text{ m}^2 \text{ V}^{-1} \text{ s}^{-1}.$$

2000 volts

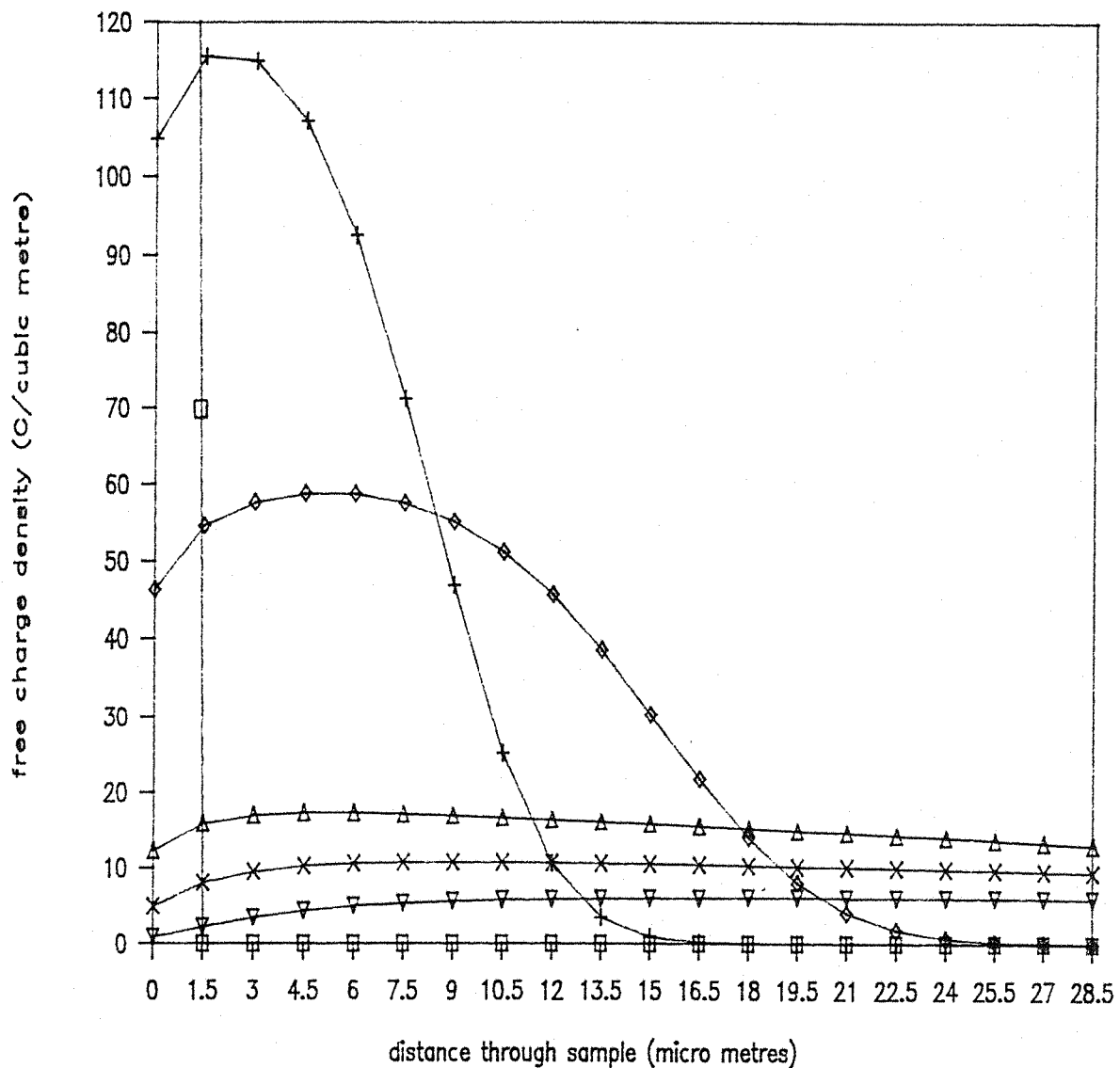


Fig. 3.14 : The free charge density distribution through the sample for different times. $\epsilon\epsilon_0 = 2 \times 10^{-11} \text{ F/m}$.

- ◻ at $t=0$ (just after the injection),
- ⊕ after 5 seconds,
- ◇ after 10 seconds,
- △ after 40 seconds,
- × after 80 seconds,
- ▽ after 160 seconds.

$$\gamma = 0.9455, T_f = 22.80 \text{ sec}, T_t = 17.70 \text{ sec}, \mu = 1.845 \times 10^{-14} \text{ m}^2 \text{ V}^{-1} \text{ s}^{-1}$$

1462 volts

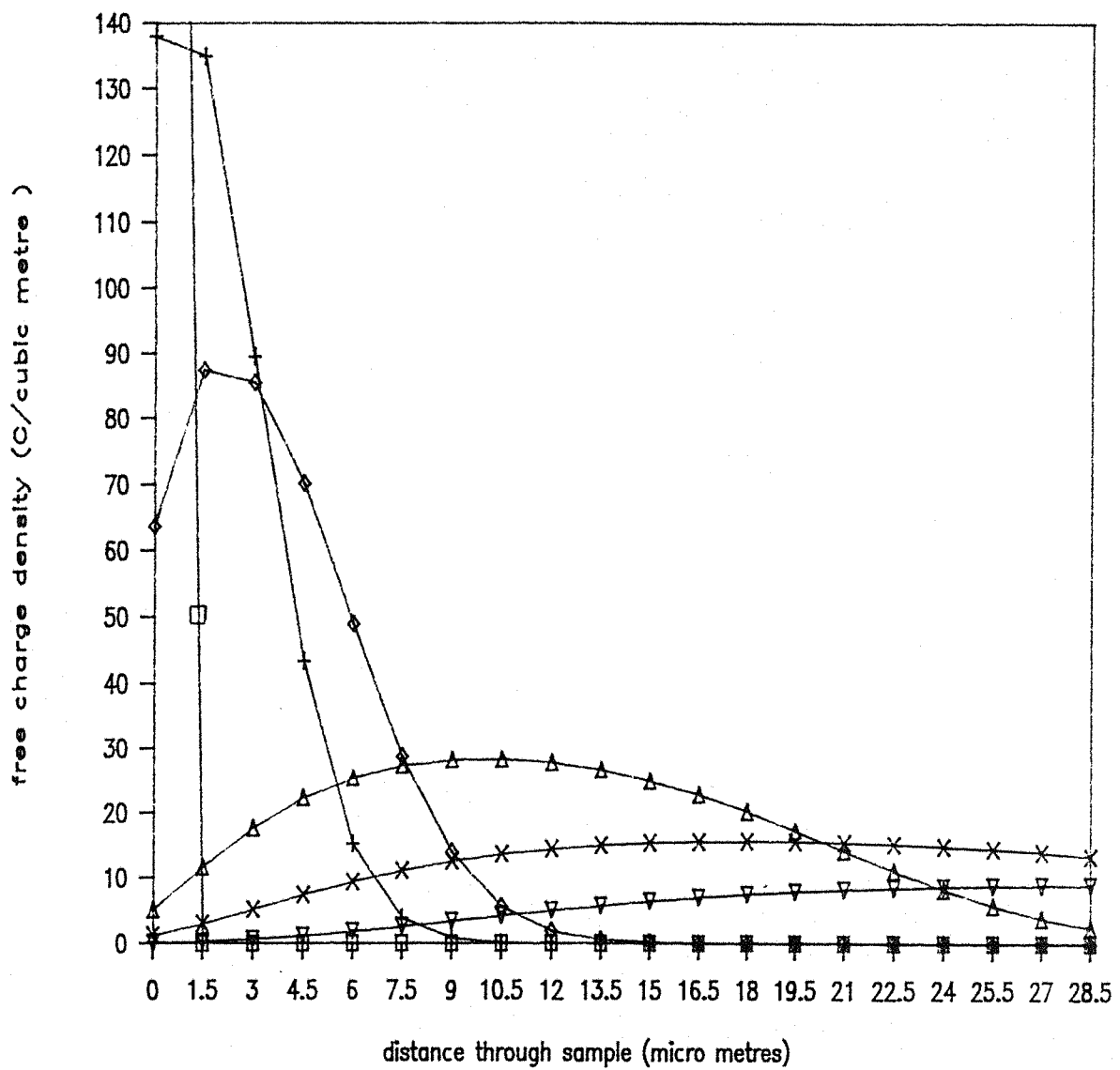


Fig. 3.15 : The free charge density distribution through the sample for different times. $\varepsilon\varepsilon_0 = 2 \times 10^{-11} \text{ F/m.}$

- at $t=0$ (just after the injection),
- ⊕ after 5 seconds,
- ◇ after 10 seconds,
- △ after 40 seconds,
- × after 80 seconds,
- ▽ after 160 seconds.

$$\gamma = 0.693, T_f = 79.44 \text{ sec}, T_t = 25.83 \text{ sec}, \mu = 9.29 \times 10^{-15} \text{ m}^2 \text{ V}^{-1} \text{ s}^{-1}.$$

492 volts

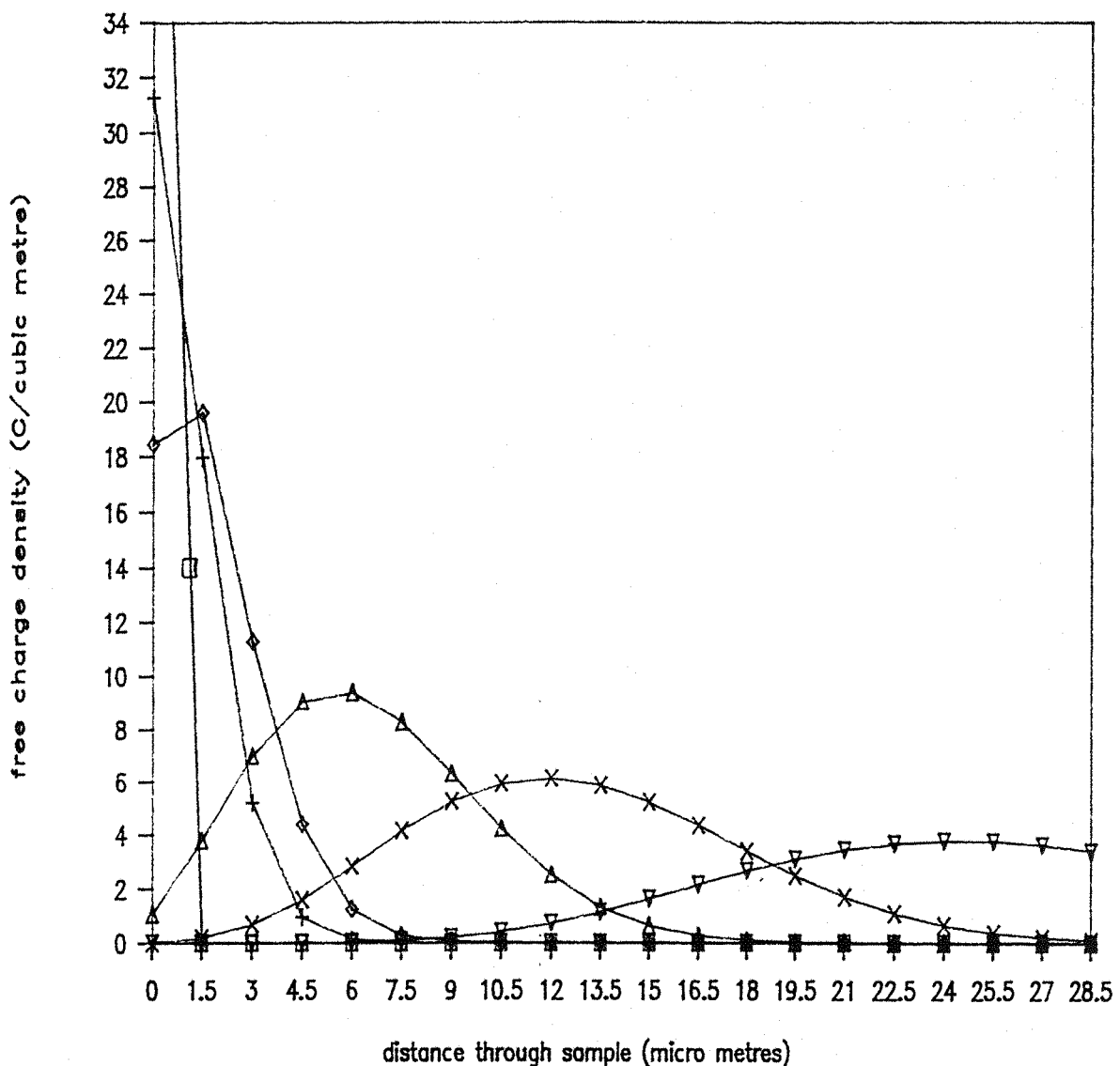


Fig. 3.17 : The free charge density distribution through the sample for different times. $\varepsilon\varepsilon_0 = 2 \times 10^{-11} \text{ F/m.}$

- at $t=0$ (just after the injection),
- ⊕ after 5 seconds,
- ◇ after 10 seconds,
- △ after 40 seconds,
- × after 80 seconds,
- ▽ after 160 seconds.

$$\gamma = 0.255, T_f = 1232.8 \text{ sec}, T_t = 5424.5 \text{ sec}, \mu = 1.095 \times 10^{-14} \text{ m}^2 \text{ V}^{-1} \text{ s}^{-1}.$$

3.2.3 The trapped charge density

At $t=0$ we assumed that there was no trapped charge in the sample. Immediately after the injection when there is an upsurge of free charge into the sample, some of the charge carriers are trapped and later released as free carriers. The values of T_f and T_t may play an important role in determining the shape of the trapped charge distributions. For the highest surface potential where the peak of the free charge distribution does not move across the sample, it is to be expected that the peak of the trapped charge density distribution would behave in a similar manner. For the lower surface potentials, where the peak of free charge distribution moves towards the opposite surface, the degree of trapping increases across the sample as shown for the two lowest surface potentials in Fig. 3.21 - 3.22.

3.2.4 The total charge in the sample

Since no recombination of charges is considered the total amount of charge in the sample must remain constant while $t < \text{transit time}$. In other words the total trapped charge (i.e. the area under the trapped charge density curve) plus the total free charge (i.e. the area under the free charge density curve) in the sample at any time less than the transit time should be constant. This is clearly demonstrated in Fig. 3.23. The calculation of the total free and trapped charge has been performed by simple summation of each distribution

2500 volts

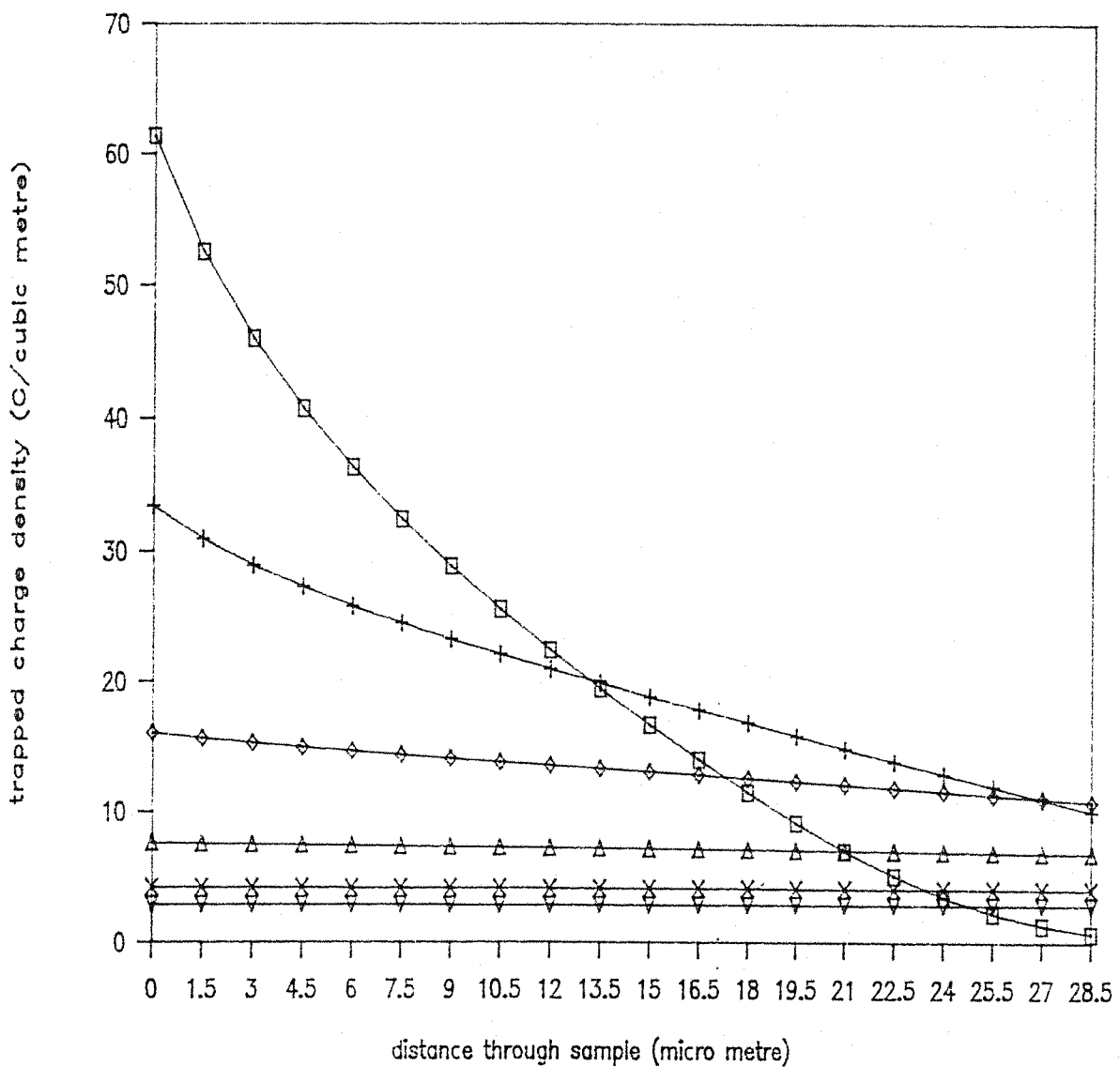


Fig. 3.18 : The trapped charge density distribution through the sample for different times

$$\varepsilon \varepsilon_0 = 2 \times 10^{-11} \text{ F/m.}$$

□ after 10 seconds,

⊕ after 20 seconds,

◇ after 40 seconds,

△ after 80 seconds,

× after 140 seconds,

▽ after 200 seconds.

$$\gamma = 1, T_f = 8.72 \text{ sec}, T_t = 6.21 \text{ sec}, \mu = 2.576 \times 10^{-14} \text{ m}^2 \text{ V}^{-1} \text{ s}^{-1}$$

2000 volts

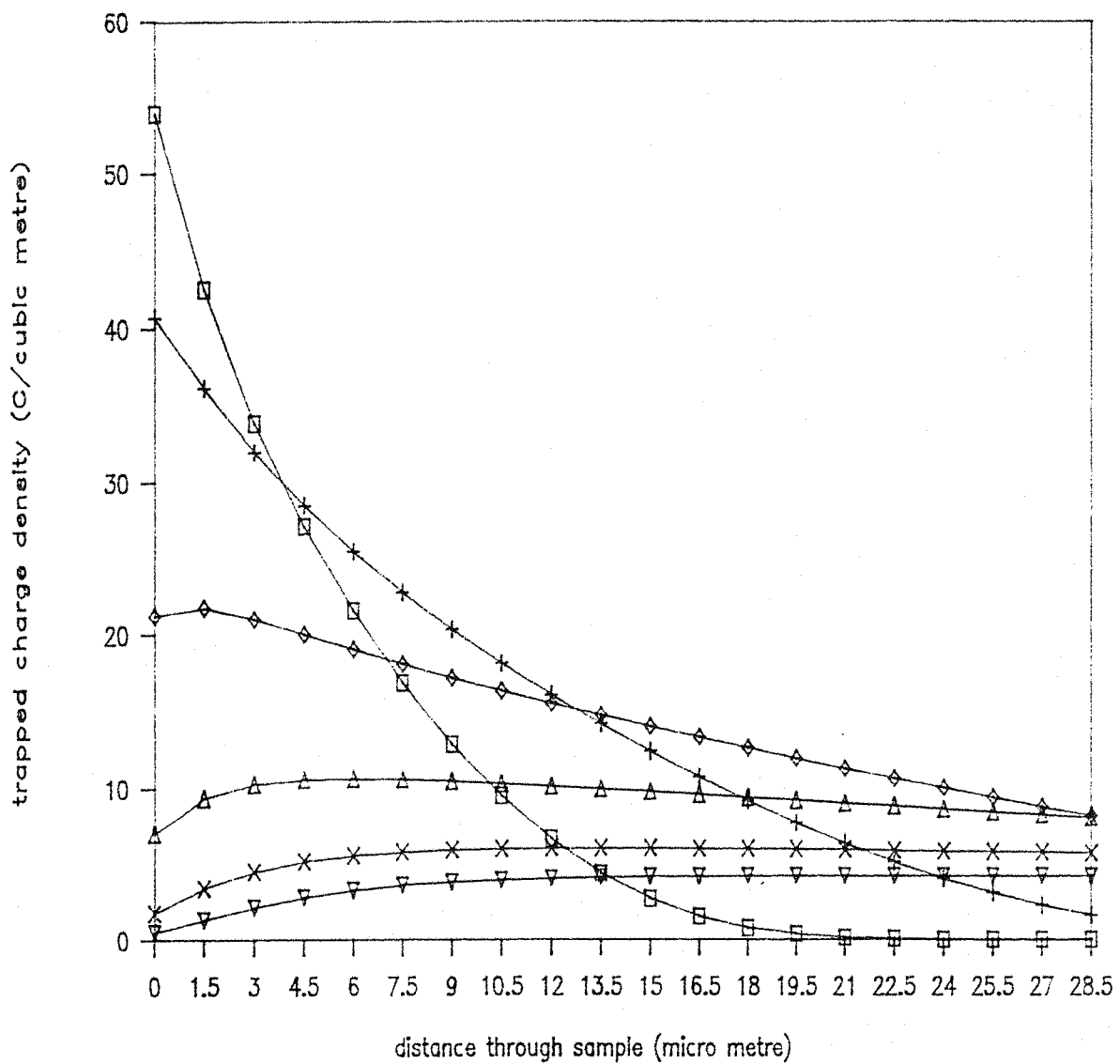


Fig. 3.19 : The trapped charge density distribution through the sample for different times

$$\epsilon \epsilon_0 = 2 \times 10^{-11} \text{ F/m.}$$

□ after 10 seconds,

+ after 20 seconds,

◊ after 40 seconds,

△ after 80 seconds,

× after 140 seconds,

▽ after 200 seconds.

$$\gamma = 0.9455, T_f = 22.80 \text{ sec}, T_t = 17.70 \text{ sec}, \mu = 1.845 \times 10^{-14} \text{ m}^2 \text{ V}^{-1} \text{ s}^{-1}.$$

1462 volts

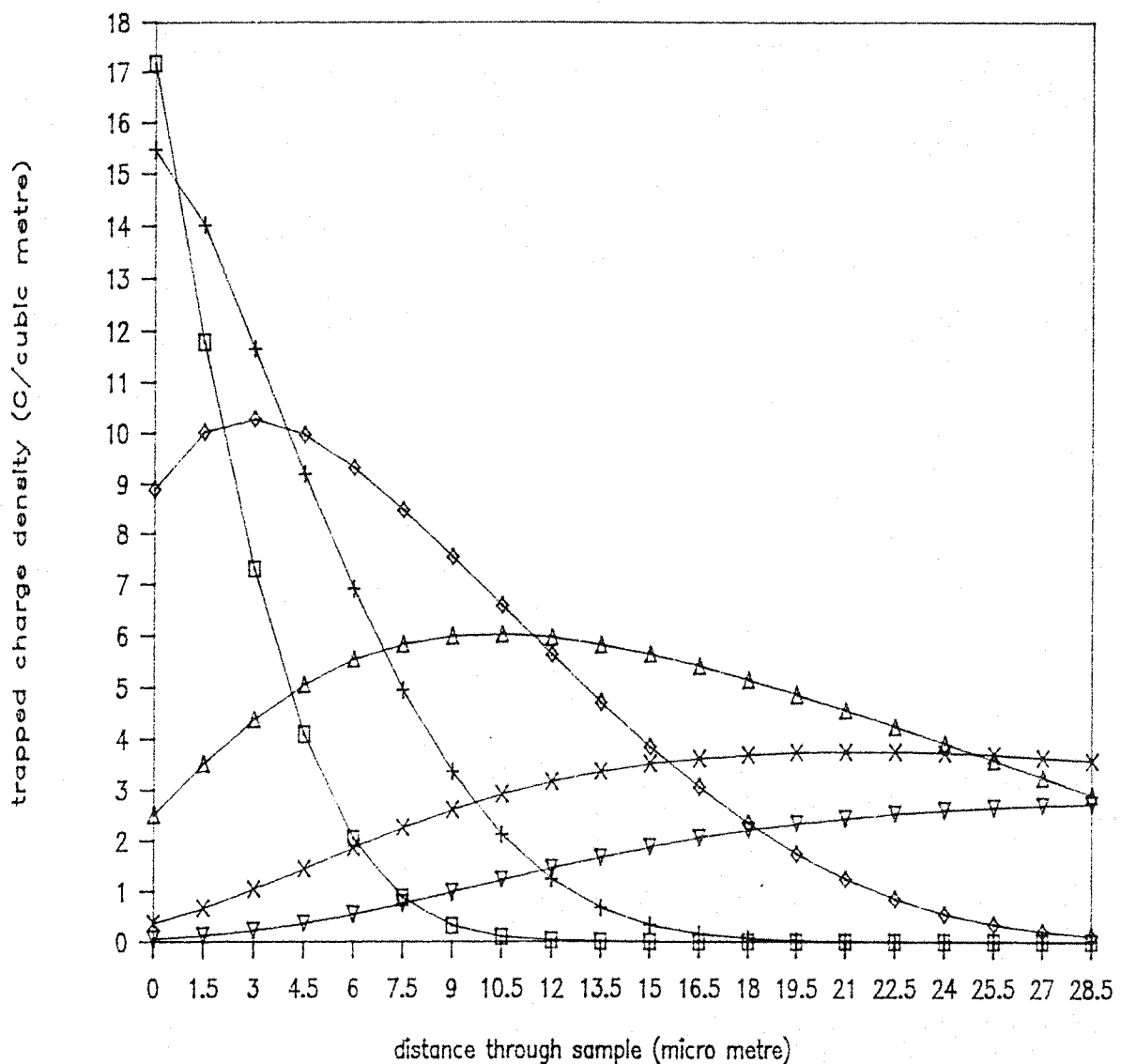


Fig. 3.20 : The trapped charge density distribution through the sample for different times

$$\epsilon \epsilon_0 = 2 \times 10^{-11} \text{ F/m.}$$

□ after 10 seconds,

⊕ after 20 seconds,

◇ after 40 seconds,

△ after 80 seconds,

× after 140 seconds,

▽ after 200 seconds.

$$\gamma = 0.693, T_f = 79.44 \text{ sec}, T_t = 25.83 \text{ sec}, \mu = 9.29 \times 10^{-15} \text{ m}^2 \text{ V}^{-1} \text{ s}^{-1}.$$

975 volts

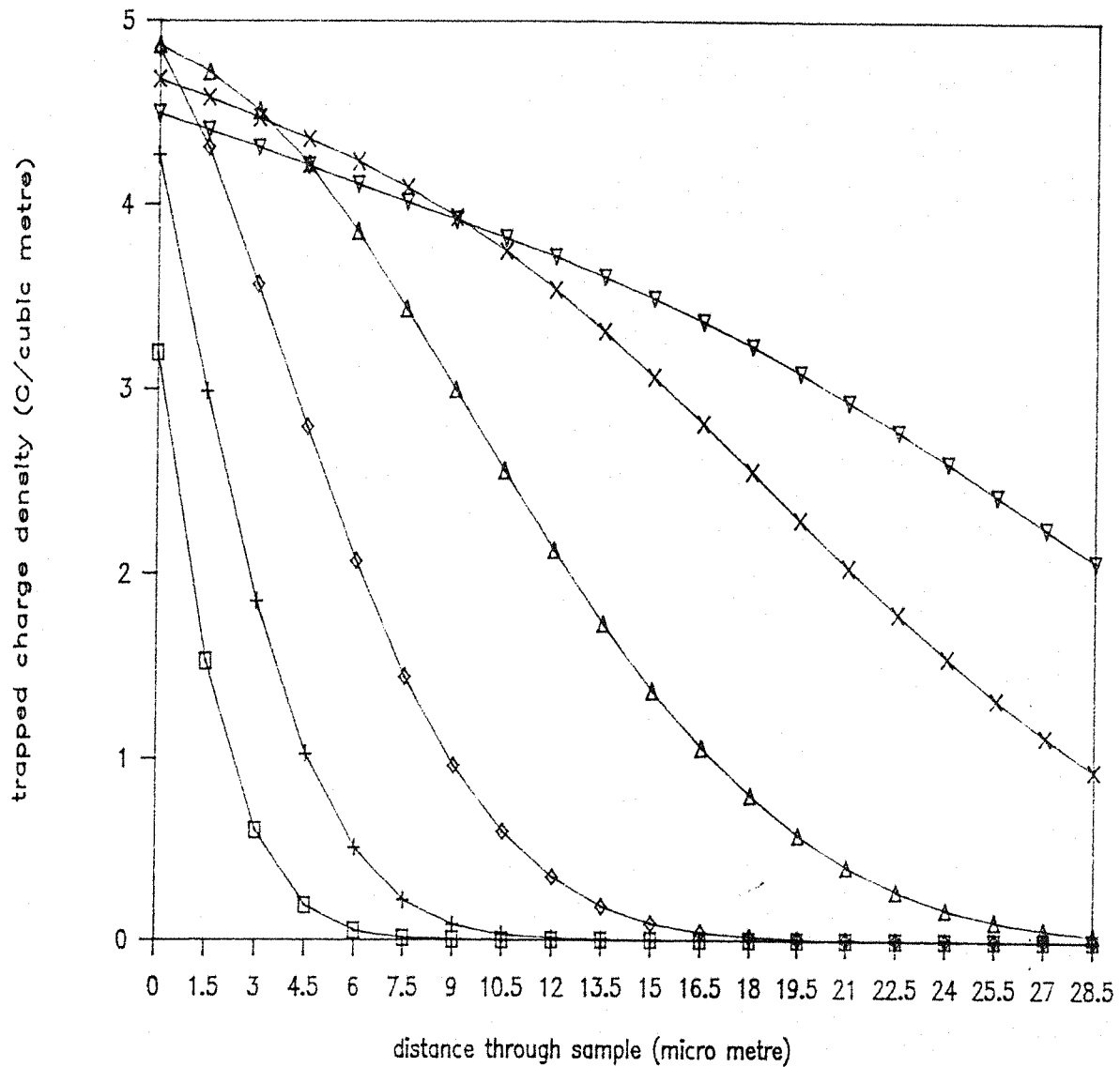


Fig. 3.21 : The trapped charge density distribution through the sample for different times

$$\varepsilon \varepsilon_0 = 2 \times 10^{-11} \text{ F/m.}$$

- \square after 10 seconds,
- $+$ after 20 seconds,
- \diamond after 40 seconds,
- \triangle after 80 seconds,
- \times after 140 seconds,
- ∇ after 200 seconds.

$$\gamma = 0.500, T_f = 372.6 \text{ sec}, T_t = 1408.8 \text{ sec}, \mu = 6.835 \times 10^{-15} \text{ m}^2 \text{ V}^{-1} \text{ s}^{-1}.$$

492 volts

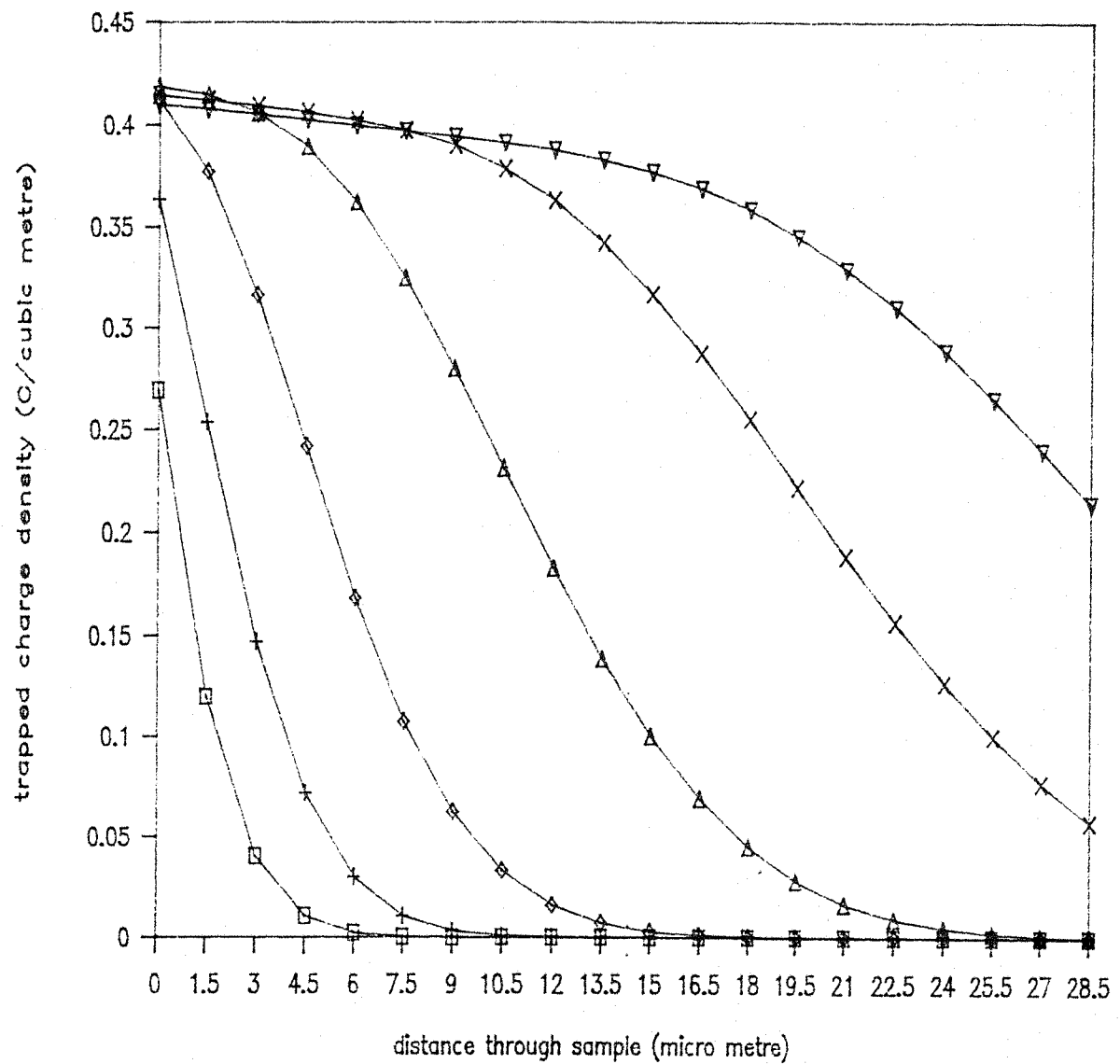


Fig. 3.22 : The trapped charge density distribution through the sample for different times

$$\varepsilon \varepsilon_0 = 2 \times 10^{-11} \text{ F/m.}$$

- after 10 seconds,
- ⊕ after 20 seconds,
- ◇ after 40 seconds,
- △ after 80 seconds,
- × after 140 seconds,
- ▽ after 200 seconds.

$$\gamma = 0.255, T_f = 1232.8 \text{ sec}, T_t = 5424.5 \text{ sec}, \mu = 1.095 \times 10^{-14} \text{ m}^2 \text{ V}^{-1} \text{ s}^{-1}$$

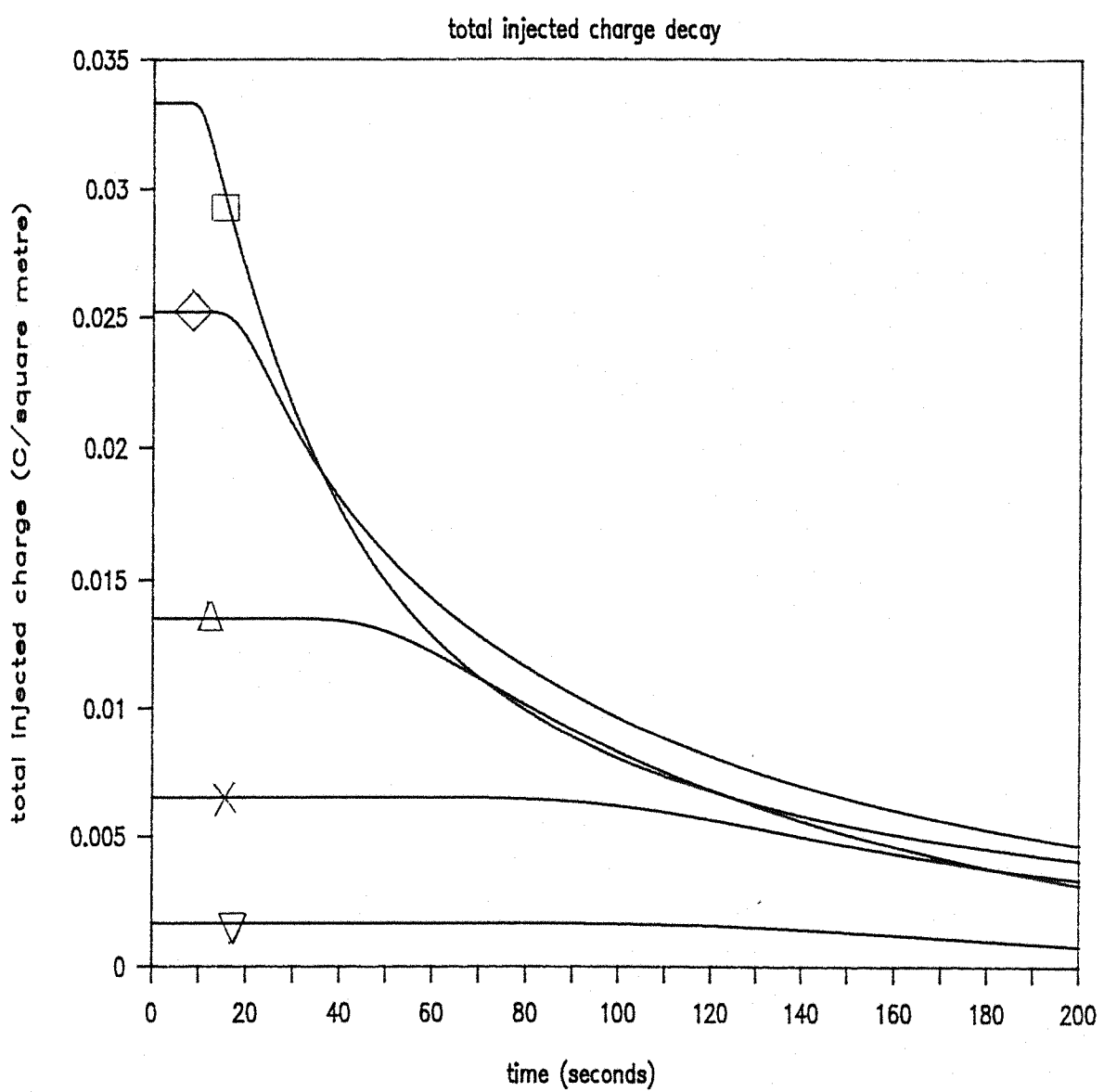


Fig. 3.23 : The total injected charge decay curves for different initial voltages using the parameters of Table 1.

$$\varepsilon \varepsilon_0 = 2 \times 10^{-11} \text{ F/m.}$$

- for 2500 volts,
- ◇ for 2000 volts,
- △ for 1462 volts,
- ✗ for 975 volts,
- ▽ for 492 volts.

(using the trapezium rule).

3.2.5 Other transport parameters

The transport parameters are directly related to the transport and trapping of carriers at the microscopic level. In our particular case we have (ref 43)

$$T_t = 1/(\nu^* \exp(-E_t/kT)), \quad (43)$$

where

ν^* is the frequency of attempts to escape,

E_t is the trap energy,

and

$$T_f = 1/((N_t - \rho_t)Sv). \quad (44)$$

where

N_t is the density of traps,

ρ_t is the trapped charge density,

S is the capture cross section of an unoccupied centre,

v is the carrier velocity ($v = \mu E$).

ν^* is often regarded as the product of the highest lattice frequency and a constant less than or equal to unity, expressing the probability that a carrier exited energetically to the transport band, and another parameter which is the ratio of states at the energies of the transport band above the ground state, (these being the number of states into which the carrier can be excited) to the number of states in the ground state. It is worth mentioning this last factor because in principle ν^* can exceed the highest lattice frequency (ref 43). However, commonly chosen values of ν^* are in the range of 10^{12} to 10^{15} s^{-1} (ref 25).

Initial surface potential(volts)	2500	2000	1462	975	492
E_t (eV)	0.97	0.99	1.002	1.102	1.136
N_t (m^{-3}) $\times 10^{23}$	5.35	3.56	2.78	2.22	0.45

Table 2. trap energy and concentration for various initial surface potentials. $v^* = 10^{15} s^{-1}$, $S = 10^{-19} m^2$,
 $T = 290$ K.

This variation in ν^* causes a variation of about 15% on the calculated values of E_t .

At the beginning of the experiment when no trapped charge exists in the sample equation (44) becomes:

$$T_f = 1/N_t S \mu E_0 \quad (45)$$

The capture cross section is taken to be $S=10^{-19} \text{ m}^2$ (ref 25).

Table 2 shows the derived values for E_t and N_t .

3.3 Discussion

The most important of the transport parameters is the injection factor γ which accounts for the crossover effect (see for example ref 25 and ref 40). The values of γ as shown in Fig. 3.24, suggest a linear field dependency for lower field values. Sonnonstine and Perlman (ref 36) assumed such a field dependency to account for the crossover effect. However, as the value of the electric field increases this linear dependency must break down at some point. The Schottky effect (field enhanced thermal detrapping, see ref 41) might be an appropriate mechanism to account for the detrapping of carriers from the surface states into the bulk states but this cannot be confirmed because not enough data exists for such an analysis.

The charge mobility values for PE appear not to fall into an obvious pattern in the range studied. However, the electric field dependency of carrier mobilities have been reported by von Berlepsch (ref 24) and Mizutani and Ieda (ref 49). The magnitudes of mobilities derived here are in the

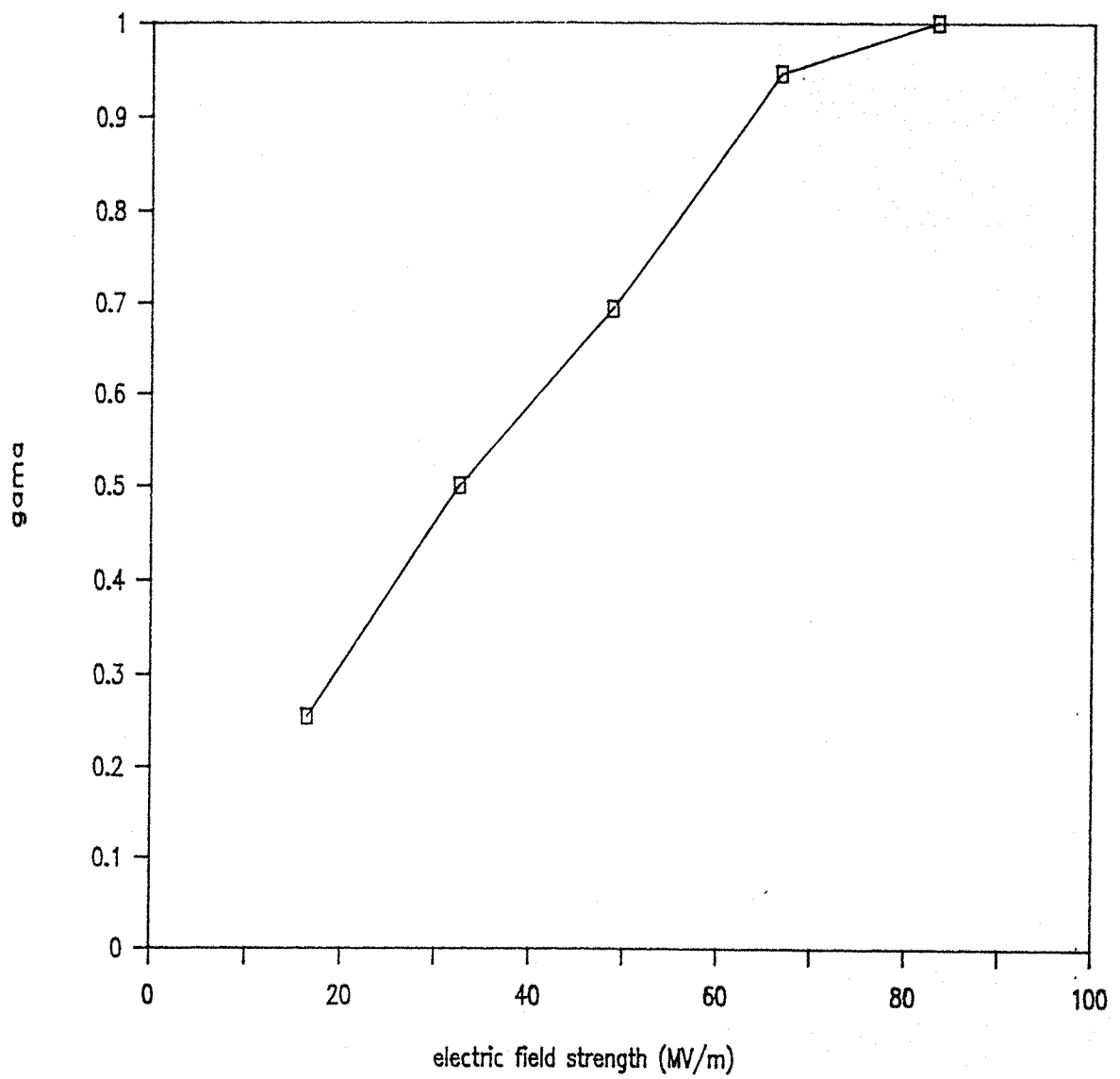


Fig. 3. 24 : Injection factor (γ) versus initial electric field.(see Table 1.)

range reported by these and other authors (see for example ref 9 and ref 25 and ref 36). Different methods of production, morphology, additives, humidity, etc..., affect the charge mobility in PE.

As indicated in Table 2 T_t and T_f show strong field dependency. Fig. 3.25 and 3.26 suggest linear dependencies between the logarithm of the electric field and the logarithms of T_f and T_t . Similar linear dependencies for T_f and T_t has also been reported by von Berlepsch (ref 25) and for other types of polymers by von Seggern (ref 7) and Chudleigh (ref 2). The values of T_f are in very good agreement with the values reported by von Berlepsch, but the values of T_t derived here are significantly smaller than the corresponding values reported by von Berlepsch.

The average trap concentration of $(2.87 \pm 1.79) \times 10^{23} \text{ m}^{-3}$ is in good agreement with the value of about $4 \times 10^{23} \text{ m}^{-3}$ reported by von Berlepsch (ref 25).

Assuming the validity of the band scheme for PE, then it is interesting to see that the trap energy value of 1.136 eV at field 16.4 MV/m is in good agreement with the peak trap energy of about 1.5 eV reported by Ieda (see Fig. 1.2), and is in the range reported by Toomer and Lewis (ref 9) and von Berlepsch (ref 25).

The effect of band lowering mechanisms (i.e. Poole-Frenkel effect) in high electric fields on trap energy has been indicated in Table 2. The amount of band lowering due to this effect is (ref 41):

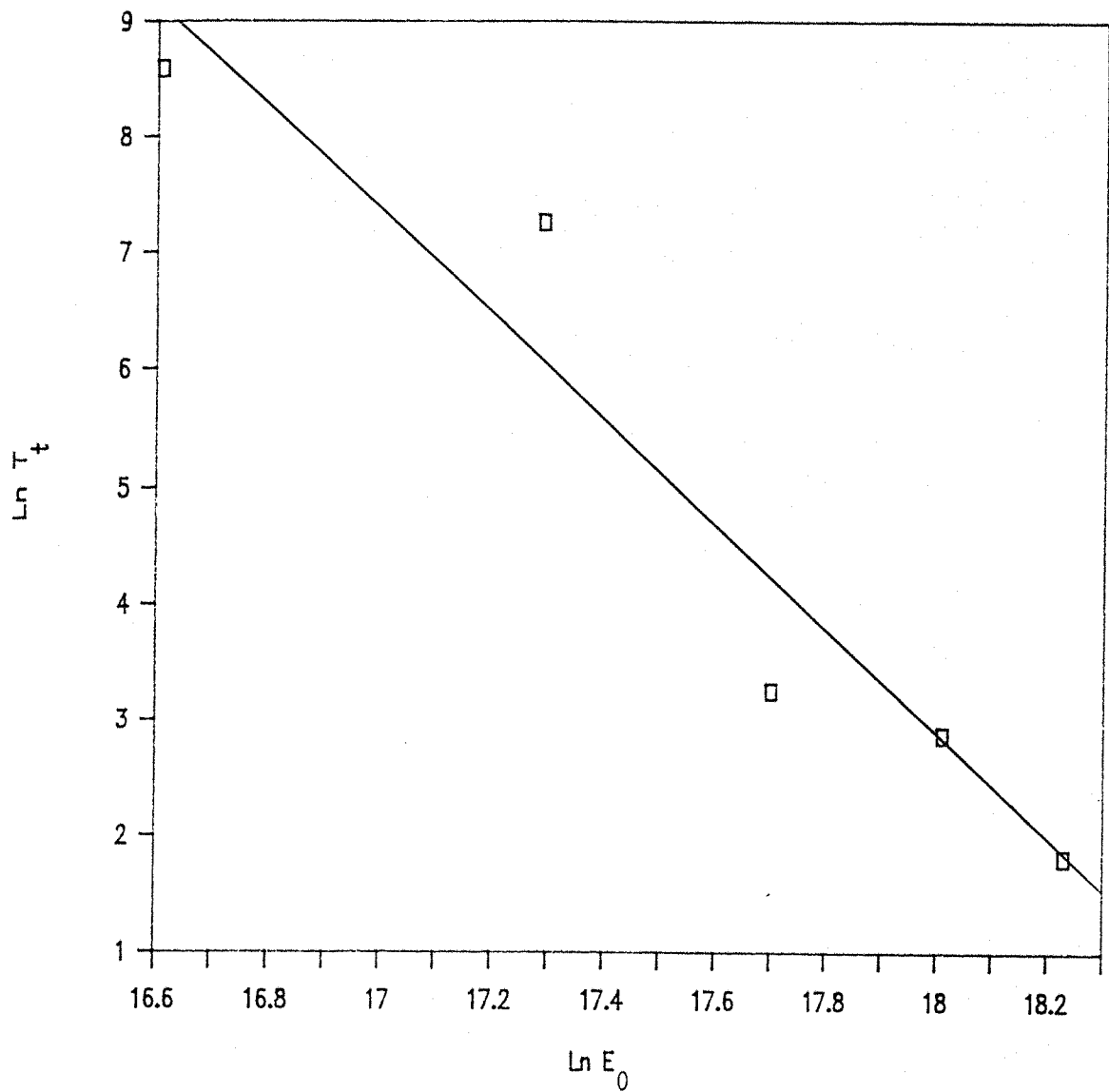


Fig. 3. 25 : Ln-Ln plot of T_t versus initial electric field.
The line is least square best fit.

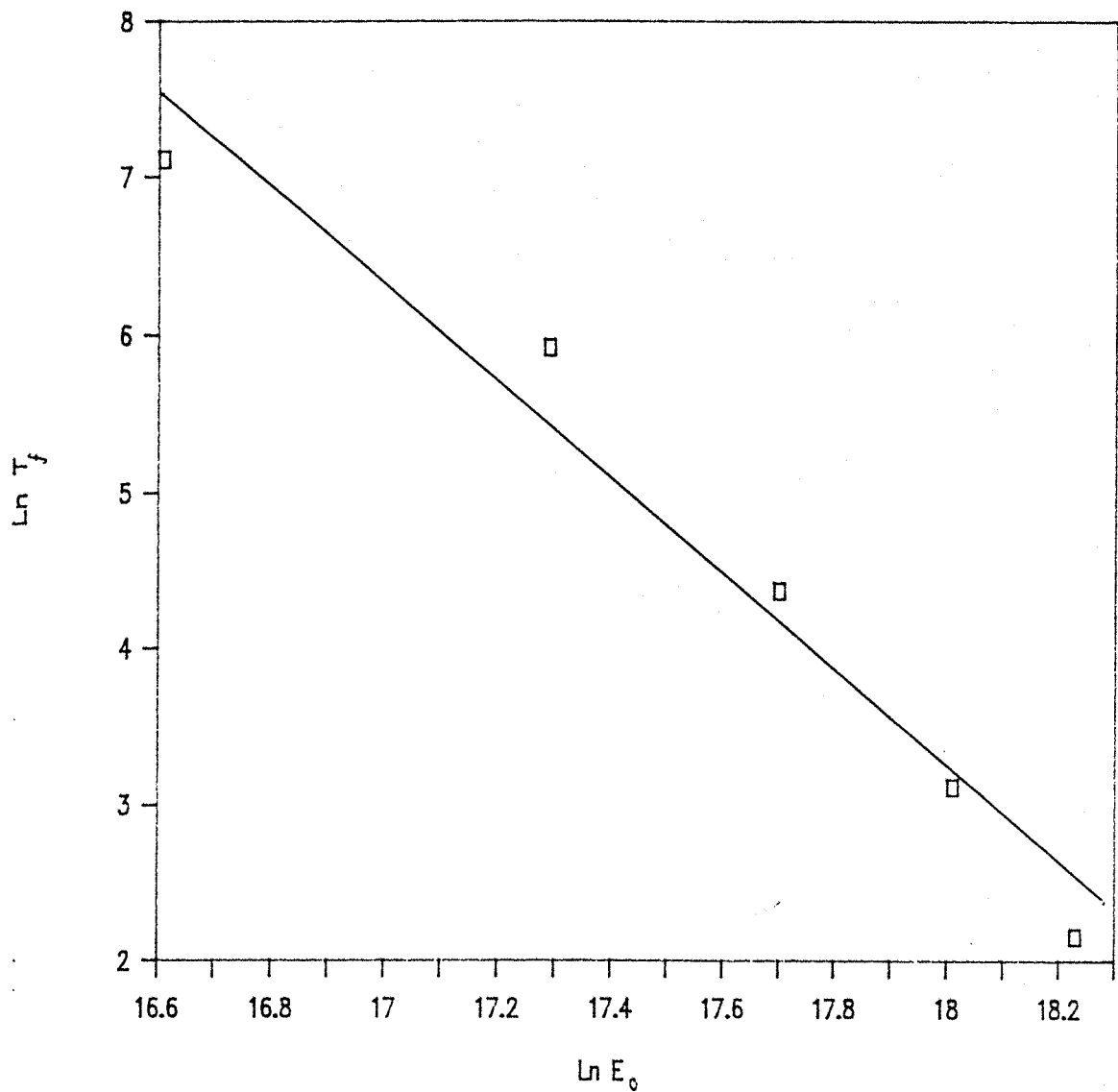


Fig. 3.26 : Ln-Ln plot of T_f versus initial electric field.

The line is least square best fit.

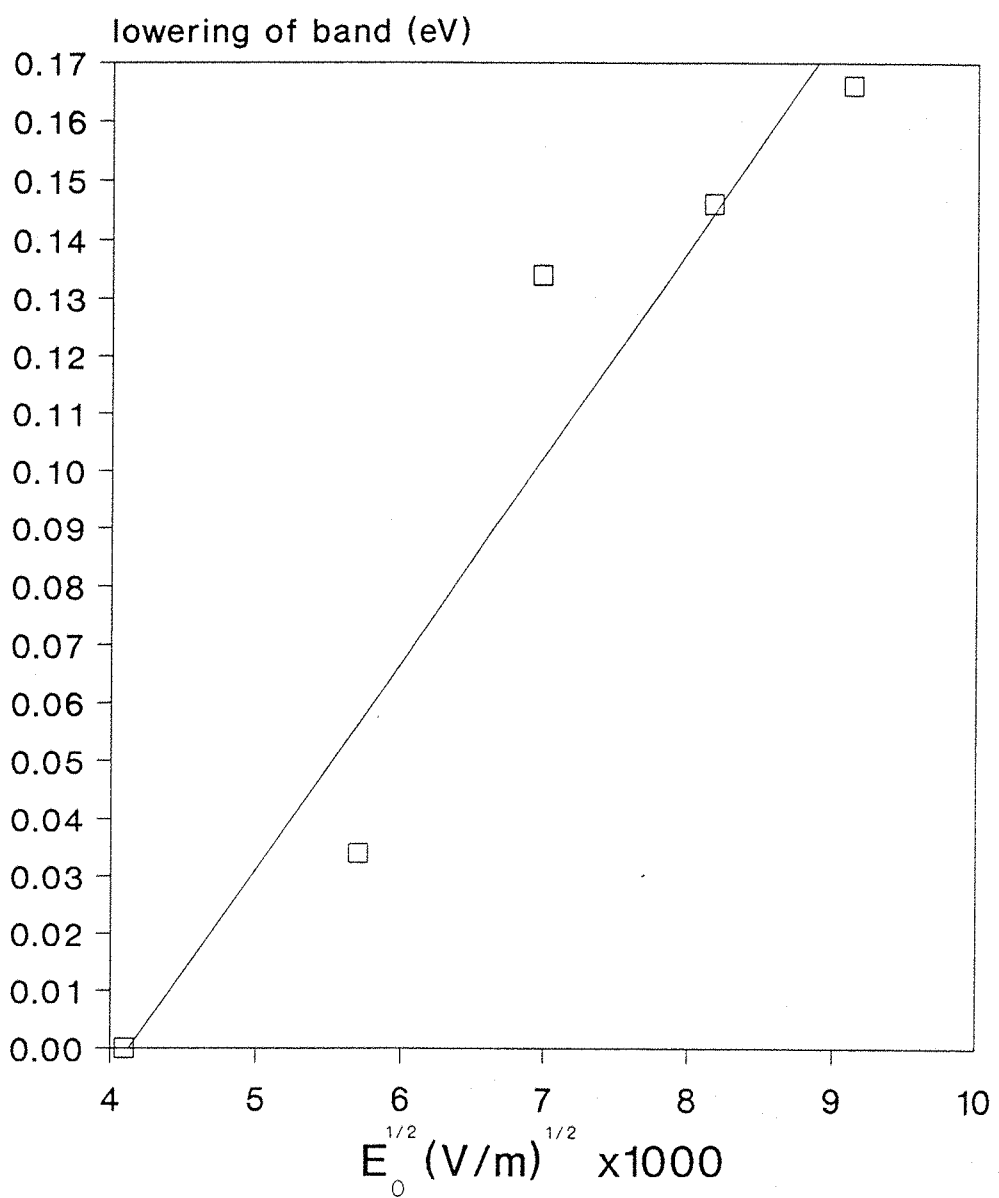


Fig. 3. 27 : Lowering of the conduction band by electric field.

The line is least square best fit. The gradient represents β_{PF} constant.

$$\Delta E_{PF} = \beta_{PF} E^{1/2}$$

where ΔE_{PF} is the amount of conduction band energy which is lowered, β_{PF} is the Poole-Frenkel constant and it is given by:

$$\beta_{PF} = (q^3 / \pi \epsilon \epsilon_0)^{1/2}$$

where q is the electronic charge. For PE where $\epsilon \epsilon_0 = 2 \times 10^{-11} \text{ F/m}$, we have:

$$\beta_{PF} = 5.04 \times 10^{-5} \text{ C V}^{1/2} \text{ m}^{1/2}$$

If we consider the trap energy of the lowest initial voltage (i.e. 492 volts) as a reference, we can plot the amount of the lowering of the band against $E_0^{1/2}$. This is shown in Fig. 3.27. Using the least-square analysis, the gradient of the line is found to be $(3.5 \pm 0.3) \times 10^{-5} \text{ C V}^{1/2} \text{ m}^{1/2}$ which is in good agreement with the calculated value of β_{PF} .

3.4 Conclusion

The proposed transport model accounts for the main features of the experimental results in terms of four transport parameters i.e. charge mobility, injection factor, trapping time and release time. The transport and trapping values, and the derived values of E_t , N_t and β_{PF} , for PE are close to independently derived values in the literature, and in this respect the model is entirely satisfactory. However, there are areas that must be investigated more thoroughly. As indicated in table 1, the values of χ^2 increase as the electric field increases which suggests that the model may

need improvement to account for high field behaviour. For example a better mechanism for surface charge injection may be time dependent charge injection and not the "instantaneous" model. Also it may be important to include a field dependent mobility rather than the field independent parameter as considered here. Another fruitful approach may be to consider multiple energy levels of the traps instead of a single energy model. The resulting transport equations may appear difficult to solve and finite difference methods may not be an appropriate approximation technique, but other numerical methods (e.g. finite elements methods) have proved to be very useful in solving complicated systems of partial differential equations.

Experimentally there is a clear need for studying decay-charge profiles on other polymer materials to explore the area of applicability of the foregoing models.

1. S.J. Fox, Journal of Applied Physics, Vol. 45, No. 2, P. 610, Feb. 1974. Decay of surface potential in electrophotography: Single-carrier case.
2. P.W. Chudleigh, Journal of Applied Physics, Vol. 48, No. 11, P. 4591, Nov. 1977. Charge transport through a polymer foil.
3. T. Mizutani, A. Oota and M. Ieda, Japanese Journal of Applied Physics, Vol. 17, No. 12, P. 2178, 1978. Surface Potential Decay of Corona-Charged High-Density Polyethylene.
4. E.A. Baum, T.J. Lewis and R. Toomer, Journal of Physics D: Applied Physics, Vol. 10, P. 487, 1977. Decay of electrical charge on polyethylene films.
5. E.A. Baum, T.J. Lewis and R. Toomer, Journal of Physics D: Applied Physics, Vol. 10, P. 2525, 1977. Further observation of the decay of surface potential of corona charged polyethylene films.
6. D.M. Taylor and T.P.T. Williams, Journal of Physics C: Solid States Physics, Vol. 11, P. 111, 1978. Decay of surface charge in the presence of a time-dependent bulk conductivity.
7. H. von Seggern, Journal of Applied Physics, Vol. 50, No. 11, P. 7039, Nov. 1979. A new model of isothermal charge transport for negatively corona-charged Teflon.
8. K.J. Kao, S.S. Bamji and M.M. Perlman, Journal of Applied Physics, Vol. 50, No. 12, P. 8181, Dec. 1979. Thermally stimulated discharge current study of surface charge release in polyethylene by corona-charged excited molecules, and the crossover phenomenon.
9. R. Toomer and T.J. Lewis, Journal of Physics D: Applied Physics, Vol. 13, P. 1343, 1980. Charge trapping in

corona-charged polyethylene films.

10. P.G. Lederer, T.J. Lewis and R. Toomer, J. Chem. Soc., Faraday Trans. 1, 1981, 77, 2989-3003. Electrical charge mobility in hydrated bovine serum albumin.
11. S. Radhakrishnan, M.N. Kamalasan, and P.C. Mehendru, Phys. Stat. Sol. (a), Vol. 68, P. 117, 1981. Surface Charge Decay Characteristics in Polyvinyl Acetate Films.
12. M. Campos and J.A. Giacometti, Journal of Applied Physics, Vol. 52, No. 7, P. 4546, July 1981. Surface-potential decay in insulators with deep traps.
13. T. Kaura and R. Nath, POLYMER, Vol.22, P. 1642, Dec 1981. Drift mobility determination using surface-charge decay technique in polyvinlidene flouoride (PVF₂).
14. C. Barnes, P.G. Lederer, T.J. Lewis and R. Toomer, Journal of Electrostatics, Vol. 10, P. 107, 1981. Electron and ion transfer processes at insulator surfaces.
16. T. Mizutani, T. Oomura and M. Ieda, Japanese Journal of Applied Physics, Vol. 20, No. 5, P. 855, May 1981. Surface Potential Decay in Polyethylene.
17. A. Kumar and R. Nath, Journal of the Physical Society of Japan, Vol. 51, No. 1, P.208, Jan. 1982. On the Theroy of Suface Charge Decay in Dielectrics.
18. A.M. Andriesh, A.I. Buzdugan, L.I. Zelenina and S.D. Shutov, Phys. Stat. Sol. (a), Vol 74, P. K79, 1982. Dark Decay of Surface Potential in Vitreous As₂S₃.
19. H. von Berlepsch and L. Brehmer, Phys. Stat. Sol. (a), Vol. 76, P. K27, 1983. Invalidity of the Scaling Property of Surface Potential Kinetics in HD PE.
20. A. Kumar and R. Nath, Journal of Electrostatics, Vol. 14, P. 201, 1983. Study of the surface potential decay characteristics in cellulose acetate films.

21. H. von Berlepsch, Phys. Stat. Sol. (a), Vol. 81, P. K63, 1984. Trapping Model for the Surface Potential Kinetics in HD PE.
22. H. Qiu, S. Xi-ming, Proc. 5th Intern. Symp. Electrets, Heidelberg 1985 (Avail. from IEEE, NY). The study of isothermal decay of surface potential in corona-charged PTFE film.
23. J.A. Giacometti, G.F. Leal Ferreira and B. Gross, Phys. Stat. Sol. (a), Vol. 88, P.297, 1985. Negative charge transport in fluorethylenepropylene by the constant current method.
24. H. von Berlepsch, Phys. Stat. Sol. (a), Vol. 90, P. K97, 1985. Electric field dependent trapping time in HD PE.
25. H. von Berlepsch, Journal of Physics D: Applied Physics, Vol. 18, P.1155, 1985. Interpretation of surface potential kinetics in HD PE by a trapping model.
26. H. von Berlepsch, Phys. Stat. Sol. (a), Vol. 92, P. 285, 1985. Field dependent injection in HD PE.
27. B.L. Sharma, J.K. Quamara and P.K.C. Pillai, Journal of Electrostatics, Vol. 18, P. 313, 1986. Photoinduced discharge characteristics of Kapton-H polymide film photoreceptors.
28. R. Coelho, L. Levy and D. Sarrail, Phys. Stat. Sol. (a), Vol. 94, P. 289, 1986. On the natural decay of corona charged insulating sheets.
29. T. Kaura and V.K. Srivastava, Journal of Electrostatics, Vol. 19, P. 45, 1987. Surface potential decay in stretched and unstretched PVDF films.
30. H.J. Wintle, Journal of Applied Physics, Vol. 41, No. 10, P. 4004, Sep 1970. Decay of Static Electrification by

Conduction Processes in Polyethylene.

31. I.P. Batra, K. Keiji Kanazawa and H. Seki, Journal of Applied Physics, Vol. 41, No. 8, P. 3416, July 1970. Discharge characteristics of photoconducting insulators.
32. I.P. Batra, K. Keiji Kanazawa, B.H. Schechtman and H. Seki, Journal of Applied Physics, Vol. 42, No. 3, P. 1124, March 1971. Charge-Carrier Dynamics Following Pulsed Photojection.
33. H.J. Wintle, Japanese Journal of Applied Physics, Vol. 10, P. 659, 1971. Decay of electric charge in insulators.
34. H.J. Wintle, Journal of Applied Physics, Vol. 43, No. 7, P. 2927 July 1972. Surface-Charge Decay in Insulators with Nonconstant Mobility and with Deep Trapping.
35. I.P. Batra and K. Keiji Kanazawa, Japanese Journal of Applied Physics, Vol. 11, P. 267, 1972. On the "Cross-Over" Effect in Surface Potential Decay.
36. T.J. Sonnonstine and M.M. Perlman, Journal of Applied Physics, Vol. 46, No. 9, P. 3975, Sep 1975. Surface-potential decay in insulators with field-dependent mobility and injection efficiency.
37. H. von Seggern, Journal of Applied Physics, Vol. 50, No. 4, P. 2817, April 1979. Identification of TSC peaks and surface-voltage stability in Teflon FEP.
38. H. von Seggern, Journal of Applied Physics, Vol. 52, No. 6, P. 4086, June 1981. Detection of surface and bulk traps.
39. M. Ieda, IEEE Transactions on Electrical Insulation Vol. EI-19, No. 3, June 1984. Electrical Conduction and Carrier Traps in Polymeric Materials.
40. V.I. Arkhipov, J.A. Popova and A.I. Rudenko, Journal of

Electrostatics, Vol. 18, P. 23, 1986. Space-charge perturbed transport in disordered dielectrics.

41. K.C. Kao, W.Hwang, Electrical transport in solids, Pergamon Press, 1981.
42. G.G. Roberts, N.Apsley and R.W. Munn, Physics Reports(Review Section of Physics Letters) 60, No. 2(1980) 59-150.
43. Albert Rose, Concepts in photoconductivity and allied problems. (Interscience Publishers), 1963.
44. G.D. Smith, Numerical Solution of Partial Differential Equations: Finite Difference Methods. Oxford University Press, 1978.
45. T. Mizutani, Y. Suzuki and M. Ieda, Journal of Applied Physics, Vol. 48, P.2408, 1977. Thermally Stimulated Currents in Polyethylene and Ethylene-Vinyl-Acetate Copolymers.
46. B.W. Robins, private communication (Physics Department, Southampton).
47. R.L. Burden, J.D. Faires and A.C. Reynolds, Numerical Analysis, Prindle, Weber and Schmidt Publisher, 1981.
48. G.L. Squires. Practical Physics, McGraw Hill, 1976.
49. T. Mizutani and M. Ieda, Journal of Physics D: Applied Physics, Vol. 12, P. 291, 1979. Carrier Transport in High Density Polyethylene.

